

# A low-cost, parameter-free, and pressure-robust enriched Galerkin method for the Stokes equations\*

Seulip Lee,<sup>†</sup> Lin Mu,<sup>‡</sup>

## Abstract

In this paper, we propose a low-cost, parameter-free, and pressure-robust Stokes solver based on the enriched Galerkin (EG) method with a discontinuous velocity enrichment function. The EG method employs the interior penalty discontinuous Galerkin (IPDG) formulation to weakly impose the continuity of the velocity function. However, the symmetric IPDG formulation, despite of its advantage of symmetry, requires a lot of computational effort to choose an optimal penalty parameter and to compute different trace terms. In order to reduce such effort, we replace the derivatives of the velocity function with its weak derivatives computed by the geometric data of elements. Therefore, our modified EG (mEG) method is a parameter-free numerical scheme which has reduced computational complexity as well as optimal rates of convergence. Moreover, we achieve pressure-robustness for the mEG method by employing a velocity reconstruction operator on the load vector on the right-hand side of the discrete system. The theoretical results are confirmed through numerical experiments with two- and three- dimensional examples.

**Keywords:** enriched Galerkin finite element methods; viscous Stokes equations; interior penalty methods; weak derivatives; parameter-free; pressure-robust.

## 1 Introduction

We consider the Stokes equations in a bounded domain  $\Omega \subset \mathbb{R}^d$  for  $d = 2, 3$  with simply connected Lipschitz boundary  $\partial\Omega$ : Find fluid velocity  $\mathbf{u} : \Omega \rightarrow \mathbb{R}^d$  and pressure  $p : \Omega \rightarrow \mathbb{R}$  such that

$$-\nu\Delta\mathbf{u} + \nabla p = \mathbf{f} \quad \text{in } \Omega, \quad (1.1a)$$

$$\nabla \cdot \mathbf{u} = 0 \quad \text{in } \Omega, \quad (1.1b)$$

$$\mathbf{u} = 0 \quad \text{on } \partial\Omega, \quad (1.1c)$$

where  $\nu > 0$  is a constant fluid viscosity, and  $\mathbf{f}$  is a given body force.

In the finite element framework, finite dimensional velocity and pressure spaces must satisfy the discrete inf-sup stability condition [3, 6, 18] to guarantee the well-posedness of the discrete problem corresponding to (1.1). Various mixed finite element methods (FEMs) have been developed under the discrete inf-sup condition, such as conforming and non-conforming mixed FEMs [4, 11, 28], discontinuous Galerkin methods [15, 16], weak Galerkin methods [25, 30], and enriched Galerkin methods [7, 33]. These methods have been widely used for numerical simulations of the Stokes equations while providing their different advantages.

For the Stokes equations, discontinuous Galerkin (DG) methods have received attention as advanced numerical methods which have locally conservative divergence-free condition and geometric flexibility on meshes. The interior penalty discontinuous Galerkin (IPDG) method is an example of DG methods, and it employs penalties to impose weakly the continuity of the solutions and boundary conditions. The penalty formulation has been also adopted in enriched Galerkin methods for the Poisson equation [19, 27] and  $C^0$  interior penalty methods for the biharmonic equation [5]. Even though the IPDG method has been widely applied in numerical PDE solvers, it has been criticized for the difficulty of choosing proper penalty parameters. It is well-known that a sufficiently large penalty parameter is required to ensure the stability in the symmetric IPDG method. However, in numerical simulations, a large penalty parameter may cause the increased condition number of the stiffness matrix, which leads to inaccurate

---

\*Submitted to the editors in 2022.

<sup>†</sup>Department of Mathematics, University of Georgia, Athens, GA 30602 ([seulip.lee@uga.edu](mailto:seulip.lee@uga.edu))

<sup>‡</sup>Department of Mathematics, University of Georgia, Athens, GA 30602 ([linmu@uga.edu](mailto:linmu@uga.edu))

simulation results. Also, the lower bounds for penalty parameters [1, 2, 13] does not seem practical for general meshes because the bounds depend on the angles of the mesh elements. Therefore, we pay special attention to constructing a parameter-free scheme to resolve the difficulty on penalty parameters. Various parameter-free DG methods have been introduced for second-order elliptic problems by introducing extra degrees of freedom on edges/faces and auxiliary variables, e.g., hybrid high-order (HHO) methods [12], hybridizable discontinuous Galerkin (HDG) methods [10], and weak Galerkin (WG) methods [29]. By rewriting DG basis functions in the WG framework, another parameter-free DG method [31], which is called a modified WG method, has been developed without increasing degrees of freedom. Our work is inspired by this idea.

Our main goal in this paper is to develop a low-cost and parameter-free Stokes solver with the optimal rates in convergence. The enriched Galerkin (EG) velocity and pressure spaces have been presented in [33] for solving the Stokes equations with minimal number of degrees of freedom. The velocity space consists of linear Lagrange polynomials enriched by a discontinuous, piecewise linear, and mean-zero vector function per element, while the pressure is approximated by piecewise constant functions. That is, a velocity function  $\mathbf{v}$  can be expressed as  $\mathbf{v} = \mathbf{v}^C + \mathbf{v}^D$ , where  $\mathbf{v}^C$  is a continuous linear Lagrange polynomial and  $\mathbf{v}^D$  is a discontinuous piecewise linear enrichment function. Compared to the previous EG method [33] using the IPDG formulation, our modified EG (mEG) method is developed by replacing the derivatives of velocity functions with their weak derivatives [24]. The weak derivatives are locally computed in each element by integration by parts using the interior function  $\mathbf{v}$  and the average of  $\mathbf{v}$  along edges/faces (details will be provided in Section 3). The weak derivatives for  $\mathbf{v}^C$  remain the same as  $\nabla \mathbf{v}^C$  and  $\nabla \cdot \mathbf{v}^C$ . For the discontinuous components  $\mathbf{v}^D$ , the weak derivatives are computed as piecewise constant functions by using the geometric data of each element, e.g., vertices, edges/faces, and area/volume. In the mEG method, the bilinear forms are simply assembled by the  $L^2$ -inner product of the weak derivatives and a parameter-free penalty term. The other trace terms in the IPDG formulation are not needed. Thus, the mEG method is parameter-free, and its implementation is guaranteed to require reduced computational complexity. In the theoretical part, the coercivity and continuity of the bilinear form for the diffusion term in (1.1a) hold true with no penalty parameter. Since the bilinear form for the divergence term (1.1b) remains the same as the previous EG method, the discrete inf-sup condition of the mEG method can be inherited from the previous one. Through two- and three-dimensional examples, we compare the numerical performance of our modified EG method and the previous EG method with different penalty parameters. The numerical results demonstrate that our mEG method shows uniform stability and outperforms the previous method.

Pressure-robustness is an important property of numerical methods for the Stokes equations in the case of small viscosity  $\nu \ll 1$ . In the case, inf-sup stable pairs may not guarantee accurate numerical velocity solutions. More precisely, in standard mixed FEMs including the EG method [33], the velocity error bounds are coupled with a pressure term which is inversely proportional to the viscosity  $\nu$ . Thus, the numerical simulation for velocity may be destroyed by the factor  $1/\nu$ . In contrast, pressure-robust schemes can eliminate the pressure term from the velocity error bounds in the error estimates, so they guarantee accurate numerical velocity and pressure simultaneously. In some mixed FEMs, the pressure-robustness has been achieved by applying a velocity reconstruction operator [21] to the load vector on the right hand side (see [14, 17, 20, 22, 23, 26, 35] as examples). To develop a pressure-robust scheme corresponding to the mEG method, we employ the velocity reconstruction operator [17] mapping the velocity test function into the first-order Brezzi-Douglas-Marini space. Therefore, the pressure-robustness in the mEG method is achieved without compromising the optimal rates in convergence.

The remaining sections of this paper are structured as follows: Some important definitions, notations, and trace properties are introduced in Section 2. In Section 3, we recall the EG method [33] and propose the modified EG (mEG) method without a penalty parameter. In Section 4, we prove well-posedness and error estimates of our mEG method. A pressure-robust mEG method is presented and its robust error estimates are proved in Section 5. In Section 6, we validate our theoretical results through numerical experiments in two and three dimensions. We summarize our contribution in this paper and discuss related future research in Section 7.

## 2 Preliminaries

To begin with, we introduce some notations and definitions used throughout this paper. For a bounded Lipschitz domain  $\mathcal{D} \in \mathbb{R}^d$ , where  $d = 2, 3$ , we denote the Sobolev space as  $H^s(\mathcal{D})$  for a real number  $s \geq 0$ . Its norm and seminorm are denoted by  $\|\cdot\|_{s,\mathcal{D}}$  and  $|\cdot|_{s,\mathcal{D}}$ , respectively. The space  $H^0(\mathcal{D})$  coincides with  $L^2(\mathcal{D})$ , and the  $L^2$ -inner product is denoted by  $(\cdot, \cdot)_{\mathcal{D}}$ . When  $\mathcal{D} = \Omega$ , the subscript  $\mathcal{D}$  will be omitted.

These notations are generalized to vector- and tensor-valued Sobolev spaces. The notation  $H_0^1(\mathcal{D})$  means the space of  $v \in H^1(\mathcal{D})$  such that  $v = 0$  on  $\partial\mathcal{D}$ , and  $L_0^2(\mathcal{D})$  means the space of  $v \in L^2(\mathcal{D})$  such that  $(v, 1)_{\mathcal{D}} = 0$ . The polynomial spaces of degree less than or equal to  $k$  are denoted as  $P_k(\mathcal{D})$ .

For discrete schemes, we assume that there exists a shape-regular triangulation  $\mathcal{T}_h$  of  $\Omega$  whose elements  $T \in \mathcal{T}_h$  are triangles in two dimensions and tetrahedrons in three dimensions. Then,  $\mathcal{E}_h$  denotes the collection of all edges/faces in  $\mathcal{T}_h$ , and  $\mathcal{E}_h = \mathcal{E}_h^o \cup \mathcal{E}_h^b$ , where  $\mathcal{E}_h^o$  is the collection of all the interior edges/faces and  $\mathcal{E}_h^b$  is that of the boundary edges/faces. For each element  $T \in \mathcal{T}_h$ , let  $h_T$  denote the diameter of  $T$  and  $\mathbf{n}_T$  (or  $\mathbf{n}$ ) denote the outward unit normal vector on  $\partial T$ . For each interior edge/face  $e \in \mathcal{E}_h^o$  shared by two adjacent elements  $T^+$  and  $T^-$ , we let  $\mathbf{n}_e$  be the unit normal vector from  $T^+$  to  $T^-$ . For each  $e \in \mathcal{E}_h^b$ ,  $\mathbf{n}_e$  denotes the outward unit normal vector on  $\partial\Omega$ .

In a shape-regular triangulation  $\mathcal{T}_h$ , the broken Sobolev space is defined as

$$H^s(\mathcal{T}_h) = \{v \in L^2(\Omega) : v|_T \in H^s(T), \forall T \in \mathcal{T}_h\},$$

equipped with the norm

$$\|v\|_{s, \mathcal{T}_h} = \left( \sum_{T \in \mathcal{T}_h} \|v\|_{s, T}^2 \right)^{1/2}.$$

When  $s = 0$ , the  $L^2$ -inner product on  $\mathcal{T}_h$  is denoted by  $(\cdot, \cdot)_{\mathcal{T}_h}$ . Also, the  $L^2$ -inner product on  $\mathcal{E}_h$  is denoted as  $\langle \cdot, \cdot \rangle_{\mathcal{E}_h}$ , and the  $L^2$ -norm on  $\mathcal{E}_h$  is defined as

$$\|v\|_{0, \mathcal{E}_h} = \left( \sum_{e \in \mathcal{E}_h} \|v\|_{0, e}^2 \right)^{1/2}.$$

The piecewise polynomial space corresponding to the broken Sobolev space is defined as

$$P_k(\mathcal{T}_h) = \{v \in L^2(\Omega) : v|_T \in P_k(T), \forall T \in \mathcal{T}_h\}.$$

In addition, the jump and average of  $v$  on  $e \in \mathcal{E}_h$  are defined as

$$[v] = \begin{cases} v^+ - v^- & \text{on } e \in \mathcal{E}_h^o, \\ v & \text{on } e \in \mathcal{E}_h^b, \end{cases} \quad \{v\} = \begin{cases} (v^+ + v^-)/2 & \text{on } e \in \mathcal{E}_h^o, \\ v & \text{on } e \in \mathcal{E}_h^b, \end{cases}$$

where  $v^\pm$  is the trace of  $v|_{T^\pm}$  on  $e \in \partial T^+ \cap \partial T^-$ . These definitions are extended to vector- and tensor-valued functions.

We also introduce the trace properties mainly used in this paper. For any vector function  $\mathbf{v}$  and scalar function  $q$ , we have

$$\sum_{T \in \mathcal{T}_h} \langle \mathbf{v} \cdot \mathbf{n}, q \rangle_{\partial T} = \langle [\mathbf{v}] \cdot \mathbf{n}_e, \{q\} \rangle_{\mathcal{E}_h} + \langle \{\mathbf{v}\} \cdot \mathbf{n}_e, [q] \rangle_{\mathcal{E}_h^o}. \quad (2.1)$$

For any function  $v \in H^1(T)$ , the following trace inequality holds

$$\|v\|_{0, e}^2 \leq C (h_T^{-1} \|v\|_{0, T}^2 + h_T \|\nabla v\|_{0, T}^2). \quad (2.2)$$

### 3 A Modified Enriched Galerkin Method

We consider the weak formulation for the Stokes problem (1.1): Find  $(\mathbf{u}, p) \in [H_0^1(\Omega)]^d \times L_0^2(\Omega)$  such that

$$\nu(\nabla \mathbf{u}, \nabla \mathbf{v}) - (\nabla \cdot \mathbf{v}, p) = (\mathbf{f}, \mathbf{v}), \quad \forall \mathbf{v} \in [H_0^1(\Omega)]^d, \quad (3.1a)$$

$$(\nabla \cdot \mathbf{u}, q) = 0, \quad \forall q \in L_0^2(\Omega). \quad (3.1b)$$

We recall the EG method [33] with its finite dimensional velocity and pressure spaces, and then introduce weak derivatives to establish the modified EG method in this section.

### 3.1 Standard enriched Galerkin method with interior penalty

We first introduce the EG finite dimensional velocity and pressure spaces. Let us denote the space of continuous components for velocity as

$$\mathbf{C}_h = \{\mathbf{v}^C \in [H_0^1(\Omega)]^d : \mathbf{v}^C|_T \in [P_1(T)]^d, \forall T \in \mathcal{T}_h\}.$$

The space of discontinuous components for velocity is defined as

$$\mathbf{D}_h = \{\mathbf{v}^D \in L^2(\Omega) : \mathbf{v}^D|_T = c(\mathbf{x} - \mathbf{x}_T), c \in \mathbb{R}, \forall T \in \mathcal{T}_h\},$$

where  $\mathbf{x}_T$  is the barycenter of  $T \in \mathcal{T}_h$ . Then, the EG finite dimensional velocity space is defined as

$$\mathbf{V}_h = \mathbf{C}_h \oplus \mathbf{D}_h,$$

that is, any function  $\mathbf{v} \in \mathbf{V}_h$  consists of unique continuous and discontinuous components,  $\mathbf{v} = \mathbf{v}^C + \mathbf{v}^D$  for  $\mathbf{v}^C \in \mathbf{C}_h$  and  $\mathbf{v}^D \in \mathbf{D}_h$ . At the same time, the EG pressure space is chosen as

$$Q_h = \{q \in L_0^2(\Omega) : q|_T \in P_0(T), \forall T \in \mathcal{T}_h\}.$$

Therefore, the EG method [33] is formulated with the pair of the spaces  $\mathbf{V}_h \times Q_h$ .

---

#### Algorithm 1 Enriched Galerkin (EG) method

---

Find  $(\mathbf{u}_h, p_h) \in \mathbf{V}_h \times Q_h$  such that

$$\mathbf{a}(\mathbf{u}_h, \mathbf{v}) - \mathbf{b}(\mathbf{v}, p_h) = (\mathbf{f}, \mathbf{v}), \quad \forall \mathbf{v} \in \mathbf{V}_h, \quad (3.2a)$$

$$\mathbf{b}(\mathbf{u}_h, q) = 0, \quad \forall q \in Q_h, \quad (3.2b)$$

where

$$\begin{aligned} \mathbf{a}(\mathbf{w}, \mathbf{v}) := & \nu((\nabla \mathbf{w}, \nabla \mathbf{v})_{\mathcal{T}_h} - \langle \{\nabla \mathbf{w}\} \cdot \mathbf{n}_e, [\mathbf{v}] \rangle_{\mathcal{E}_h} \\ & - \langle \{\nabla \mathbf{v}\} \cdot \mathbf{n}_e, [\mathbf{w}] \rangle_{\mathcal{E}_h} + \rho \langle h_e^{-1} [\mathbf{w}], [\mathbf{v}] \rangle_{\mathcal{E}_h}), \end{aligned} \quad (3.3a)$$

$$\mathbf{b}(\mathbf{w}, q) := (\nabla \cdot \mathbf{w}, q)_{\mathcal{T}_h} - \langle [\mathbf{w}] \cdot \mathbf{n}_e, \{q\} \rangle_{\mathcal{E}_h}. \quad (3.3b)$$

Here,  $\rho > 0$  is a penalty parameter and  $h_e = |e|^{1/(d-1)}$ , where  $|e|$  is the length/area of the edge/face  $e \in \mathcal{E}_h$ .

---

In the EG method, the interior penalty discontinuous Galerkin (IPDG) formulation is adopted to weakly impose the continuity of the discontinuous component  $\mathbf{v}^D \in \mathbf{D}_h$ , and it requires a sufficiently large penalty parameter  $\rho$  to guarantee the well-posedness of the method.

### 3.2 Modified enriched Galerkin method with weak derivatives

We introduce a weak Galerkin (WG) finite element space for velocity [30],

$$\mathcal{V}_h = \{\mathbf{v} = \{\mathbf{v}_0, \mathbf{v}_b\} \mid \mathbf{v}_0|_T \in [P_1(T)]^d, \forall T \in \mathcal{T}_h, \mathbf{v}_b|_e \in [P_1(e)]^d, \forall e \in \mathcal{E}_h\}.$$

Then, the EG velocity  $\mathbf{v} \in \mathbf{V}_h$  can be viewed as a WG function in  $\mathcal{V}_h$ , that is,

$$\mathbf{v}_0 = \mathbf{v}, \quad \mathbf{v}_b = \{\mathbf{v}\} \quad \Rightarrow \quad \{\mathbf{v}, \{\mathbf{v}\}\} \in \mathcal{V}_h,$$

and the weak derivatives for  $\mathbf{v} \in \mathbf{V}_h$  are locally defined as follows.

**Definition 3.1.** The weak gradient operator [24] is defined as  $\nabla_w \mathbf{v}|_T \in [P_0(T)]^{d \times d}$  when  $\mathbf{v} = \{\mathbf{v}_0, \mathbf{v}_b\} \in \mathcal{V}_h$  satisfying

$$(\nabla_w \mathbf{v}, \mathbb{N})_T = \langle \mathbf{v}_b, \mathbb{N} \cdot \mathbf{n} \rangle_{\partial T}, \quad \forall \mathbb{N} \in [P_0(T)]^{d \times d}.$$

In a similar manner, the weak gradient for the EG velocity  $\mathbf{v} \in \mathbf{V}_h$  is defined as  $\nabla_w \mathbf{v}|_T \in [P_0(T)]^{d \times d}$  such that

$$(\nabla_w \mathbf{v}, \mathbb{N})_T = \langle \{\mathbf{v}\}, \mathbb{N} \cdot \mathbf{n} \rangle_{\partial T}, \quad \forall \mathbb{N} \in [P_0(T)]^{d \times d}.$$

Moreover, the weak divergence operator [24] for  $\mathbf{v} \in \mathbf{V}_h$  is defined as  $\nabla_w \cdot \mathbf{v}|_T \in P_0(T)$  such that

$$(\nabla_w \cdot \mathbf{v}, q)_T = \langle \{\mathbf{v}\} \cdot \mathbf{n}, q \rangle_{\partial T}, \quad \forall q \in P_0(T).$$

**Remark 3.2.** For any EG velocity function  $\mathbf{v} \in \mathbf{V}_h$ , the differences between the weak derivatives and regular derivatives are given as

$$(\nabla \mathbf{v} - \nabla_w \mathbf{v}, \mathfrak{N})_{\mathcal{T}_h} = \langle [\mathbf{v}], \{\mathfrak{N}\} \cdot \mathbf{n}_e \rangle_{\mathcal{E}_h}, \quad \forall \mathfrak{N} \in [P_0(\mathcal{T}_h)]^{d \times d}, \quad (3.4a)$$

$$(\nabla \cdot \mathbf{v} - \nabla_w \cdot \mathbf{v}, q)_{\mathcal{T}_h} = \langle [\mathbf{v}] \cdot \mathbf{n}_e, \{q\} \rangle_{\mathcal{E}_h}, \quad \forall q \in P_0(\mathcal{T}_h). \quad (3.4b)$$

These identities are simply obtained from the definition of the weak derivatives and integration by parts. Since the EG velocity consists of  $\mathbf{v}^C \in \mathbf{C}_h$  and  $\mathbf{v}^D \in \mathbf{D}_h$ , it is clear to see from (3.4) that  $\nabla_w \mathbf{v}^C = \nabla \mathbf{v}^C$ ,  $\nabla_w \cdot \mathbf{v}^C = \nabla \cdot \mathbf{v}^C$ , and the jumps of  $\mathbf{v}^D$  on  $e \in \mathcal{E}_h^o$  cause the differences. In practice, the weak gradient  $\nabla_w \mathbf{v}^D$  is locally determined by

$$(\nabla_w \mathbf{v}^D)_{i,j} = \frac{n_j}{|T|} \langle \{\mathbf{v}^D\}, \mathbf{e}_i \rangle_{\partial T}, \quad 1 \leq i, j \leq d,$$

where  $n_j$  is the  $j$ -th component of  $\mathbf{n}$  and  $\mathbf{e}_i$  is the standard unit vector whose  $i$ -th component is 1. Since  $\mathbf{v}^D|_T = c(\mathbf{x} - \mathbf{x}_T)$  is a linear function, the above line/surface integral can be simply computed by the one-point quadrature rule on each edge/face, respectively. Also, the weak divergence  $\nabla_w \cdot \mathbf{v}^D$  is the trace of  $\nabla_w \mathbf{v}^D$  from the definition, which implies no associated cost in computing the weak divergence.

Therefore, we propose the modified enriched Galerkin method which is formulated by the weak derivatives for the EG velocity  $\mathbf{v} \in \mathbf{V}_h$ .

---

**Algorithm 2** Modified enriched Galerkin (mEG) method

---

Find  $(\mathbf{u}_h, p_h) \in \mathbf{V}_h \times Q_h$  such that

$$\mathbf{a}_w(\mathbf{u}_h, \mathbf{v}) - \mathbf{b}_w(\mathbf{v}, p_h) = (\mathbf{f}, \mathbf{v}), \quad \forall \mathbf{v} \in \mathbf{V}_h, \quad (3.5a)$$

$$\mathbf{b}_w(\mathbf{u}_h, q) = 0, \quad \forall q \in Q_h, \quad (3.5b)$$

where

$$\mathbf{a}_w(\mathbf{w}, \mathbf{v}) := \nu((\nabla_w \mathbf{w}, \nabla_w \mathbf{v})_{\mathcal{T}_h} + \langle h_e^{-1}[\mathbf{w}], [\mathbf{v}] \rangle_{\mathcal{E}_h}), \quad (3.6a)$$

$$\mathbf{b}_w(\mathbf{w}, q) := (\nabla_w \cdot \mathbf{w}, q)_{\mathcal{T}_h}. \quad (3.6b)$$

In this case,  $h_e = |e|^{1/(d-1)}$ , where  $|e|$  is the length/area of the edge/face  $e \in \mathcal{E}_h$ .

---

**Remark 3.3.** There is no penalty parameter in the mEG method, while the EG method in Algorithm 1 requires a sufficiently large penalty parameter  $\rho$ . We observe the result of applying (3.4a) to (3.6a),

$$\begin{aligned} \mathbf{a}_w(\mathbf{w}, \mathbf{v}) &= \nu((\nabla \mathbf{w}, \nabla \mathbf{v})_{\mathcal{T}_h} - \langle \{\nabla \mathbf{w}\} \mathbf{n}_e, [\mathbf{v}] \rangle_{\mathcal{E}_h} \\ &\quad - \langle \{\nabla_w \mathbf{v}\} \mathbf{n}_e, [\mathbf{w}] \rangle_{\mathcal{E}_h} + \langle h_e^{-1}[\mathbf{w}], [\mathbf{v}] \rangle_{\mathcal{E}_h}). \end{aligned}$$

By comparing with  $\mathbf{a}(\cdot, \cdot)$  in (3.3a), the average of the gradient in the symmetric term of  $\mathbf{a}(\cdot, \cdot)$  is replaced by that of the weak gradient, and the bilinear form  $\mathbf{a}_w(\cdot, \cdot)$  does not depend on the penalty parameter  $\rho$  (see also [32]). In addition, the identity (3.4b) implies that for any  $\mathbf{w} \in \mathbf{V}_h$  and  $q \in Q_h$ ,

$$\mathbf{b}_w(\mathbf{w}, q) = \mathbf{b}(\mathbf{w}, q), \quad (3.7)$$

which makes it simple to prove the discrete inf-sup condition. In practice, this allows us to use the same block matrices corresponding to  $\mathbf{b}(\cdot, \cdot)$  (or  $\mathbf{b}_w(\cdot, \cdot)$ ) for both EG and mEG methods.

**Remark 3.4.** For a non-homogeneous Dirichlet boundary condition ( $\mathbf{u} = \mathbf{g}$  on  $\partial\Omega$ ), the EG velocity in (3.5) satisfies  $\mathbf{u}_h = \mathbf{u}_h^C + \mathbf{u}_h^D = \mathbf{g}$  on any  $e \in \mathcal{E}_h^b$ . We treat  $\mathbf{u}_h^C = \mathbf{g}$  as an essential boundary condition and  $\mathbf{u}_h^D = \mathbf{0}$  as a natural boundary condition. In the mEG method, the condition  $\mathbf{u}_h^D = \mathbf{0}$  is weakly applied to locally compute the weak derivatives in the elements adjoining the boundary.

## 4 Well-Posedness and Error Analysis

For the EG method [33] in Algorithm 1, the well-posedness and error estimates have been proved in terms of the energy norm in  $\mathbf{V}_h$ ,

$$\|\mathbf{v}\|_{\mathcal{E}} := \left( \|\nabla \mathbf{v}\|_{0, \mathcal{T}_h}^2 + \rho \|h_e^{-1/2}[\mathbf{v}]\|_{0, \mathcal{E}_h}^2 \right)^{\frac{1}{2}}.$$

To show the discrete inf-sup condition and a priori error estimates for the **mEG** method in Algorithm 2, we employ the theoretical results of the **EG** method. In this case, the **mEG** method includes the weak derivatives, so it requires a mesh-dependent norm corresponding to the bilinear form  $\mathbf{a}_w(\cdot, \cdot)$ ,

$$\|\mathbf{v}\| := \left( \|\nabla_w \mathbf{v}\|_{0, \mathcal{T}_h}^2 + \|h_e^{-1/2}[\mathbf{v}]\|_{0, \mathcal{E}_h}^2 \right)^{\frac{1}{2}}.$$

Then, the following norm equivalence helps to prove the theoretical results of the **mEG** method.

**Lemma 4.1.** *For any  $\mathbf{v} \in \mathbf{V}_h$ , there are positive constants  $\gamma_*$  and  $\gamma^*$  independent of  $h := \max_{T \in \mathcal{T}_h} h_T$  such that*

$$\gamma_* \|\mathbf{v}\| \leq \|\mathbf{v}\|_{\mathcal{E}} \leq \gamma^* \|\mathbf{v}\|. \quad (4.1)$$

*Proof.* We start with the relation (3.4a) while choosing  $\mathfrak{N} = \nabla_w \mathbf{v}$ ,

$$\|\nabla_w \mathbf{v}\|_{0, \mathcal{T}_h}^2 = (\nabla_w \mathbf{v}, \nabla_w \mathbf{v})_{\mathcal{T}_h} = (\nabla \mathbf{v}, \nabla_w \mathbf{v})_{\mathcal{T}_h} - \langle [\mathbf{v}], \{\nabla_w \mathbf{v}\} \cdot \mathbf{n}_e \rangle_{\mathcal{E}_h}.$$

Then, the first term is simply bounded using the Cauchy-Schwarz inequality,

$$(\nabla \mathbf{v}, \nabla_w \mathbf{v})_{\mathcal{T}_h} \leq \|\nabla \mathbf{v}\|_{0, \mathcal{T}_h} \|\nabla_w \mathbf{v}\|_{0, \mathcal{T}_h},$$

and the second term is bounded using the Cauchy-Schwarz inequality and trace inequality (2.2),

$$\begin{aligned} \langle [\mathbf{v}], \{\nabla_w \mathbf{v}\} \cdot \mathbf{n}_e \rangle_{\mathcal{E}_h} &\leq \|h_e^{-1/2}[\mathbf{v}]\|_{0, \mathcal{E}_h} \|h_e^{1/2}\{\nabla_w \mathbf{v}\}\|_{0, \mathcal{E}_h} \\ &\leq C \|h_e^{-1/2}[\mathbf{v}]\|_{0, \mathcal{E}_h} \|\nabla_w \mathbf{v}\|_{0, \mathcal{T}_h}. \end{aligned}$$

Hence, we arrive at

$$\|\nabla_w \mathbf{v}\|_{0, \mathcal{T}_h} \leq C \|\mathbf{v}\|_{\mathcal{E}},$$

which implies the lower bound in (4.1).

On the other hand, we choose  $\mathfrak{N} = \nabla \mathbf{v}$  in (3.4a) and apply the Cauchy-Schwarz inequality and (2.2) to obtain

$$\|\nabla \mathbf{v}\|_{0, \mathcal{T}_h}^2 \leq (\nabla_w \mathbf{v}, \nabla \mathbf{v})_{\mathcal{T}_h} + \langle [\mathbf{v}], \{\nabla \mathbf{v}\} \cdot \mathbf{n}_e \rangle_{\mathcal{E}_h} \leq C \|\mathbf{v}\| \|\nabla \mathbf{v}\|_{0, \mathcal{T}_h}.$$

Therefore, it is clear to see that

$$\|\nabla \mathbf{v}\|_{0, \mathcal{T}_h} \leq C \|\mathbf{v}\|_{\mathcal{E}},$$

which yields the upper bound in (4.1).  $\square$

## 4.1 Well-posedness

In this subsection, with the norm equivalence (4.1), we show the well-posedness of the **mEG** method by proving the essential properties of the bilinear forms.

**Lemma 4.2.** *There exists a positive constant  $C$  independent of  $h$  such that*

$$\sup_{\mathbf{v} \in \mathbf{V}_h} \frac{\mathbf{b}_w(\mathbf{v}, q)}{\|\mathbf{v}\|} \geq C \|q\|_0, \quad \forall q \in Q_h. \quad (4.2)$$

*Proof.* It follows from (3.7), (4.1), and the discrete inf-sup condition in [33] that

$$\sup_{\mathbf{v} \in \mathbf{V}_h} \frac{\mathbf{b}_w(\mathbf{v}, q)}{\gamma_* \|\mathbf{v}\|} \geq \sup_{\mathbf{v} \in \mathbf{V}_h} \frac{\mathbf{b}(\mathbf{v}, q)}{\|\mathbf{v}\|_{\mathcal{E}}} \geq C_{\mathcal{E}} \|q\|_0, \quad \forall q \in Q_h,$$

where  $C_{\mathcal{E}}$  is the constant for the inf-sup condition with respect to  $\|\cdot\|_{\mathcal{E}}$ .  $\square$

It is also straightforward to show the continuity of  $\mathbf{b}_w(\cdot, \cdot)$  with respect to the norm  $\|\cdot\|$  using the norm equivalence (4.1).

**Lemma 4.3.** *For any  $\mathbf{v} \in \mathbf{V}_h$  and  $q \in Q_h$ , there exists a positive constant  $C$  independent of  $h$  satisfying*

$$|\mathbf{b}_w(\mathbf{v}, q)| \leq C \|q\|_0 \|\mathbf{v}\|. \quad (4.3)$$

*Proof.* It follows from (3.7), (4.1), and the continuity of  $\mathbf{b}(\cdot, \cdot)$  in [33] that

$$|\mathbf{b}_w(\mathbf{v}, q)| = |\mathbf{b}(\mathbf{v}, q)| \leq C \|q\|_0 \|\mathbf{v}\|_{\mathcal{E}} \leq C \gamma^* \|q\|_0 \|\mathbf{v}\|. \quad \square$$

In addition, we obtain the coercivity and continuity of  $\mathbf{a}_w(\cdot, \cdot)$  with respect to  $\|\cdot\|$ . (See [24] for details.)

**Lemma 4.4.** *For any  $\mathbf{v}, \mathbf{w} \in \mathbf{V}_h$ , we have the coercivity and continuity results for  $\mathbf{a}_w(\cdot, \cdot)$ :*

$$\mathbf{a}_w(\mathbf{v}, \mathbf{v}) = \nu \|\mathbf{v}\|^2, \quad (4.4)$$

$$|\mathbf{a}_w(\mathbf{v}, \mathbf{w})| \leq \nu \|\mathbf{v}\| \|\mathbf{w}\|. \quad (4.5)$$

Thus, we obtain the well-posedness of the mEG method.

**Theorem 4.5.** *There exists a unique solution  $(\mathbf{u}_h, p_h) \in \mathbf{V}_h \times Q_h$  to the mEG method in Algorithm 2.*

*Proof.* Since  $\mathbf{V}_h$  and  $Q_h$  are finite dimensional spaces, it suffices to show that  $\mathbf{u}_h = \mathbf{0}$  and  $p_h = 0$  when  $\mathbf{f} = \mathbf{0}$ . If we choose  $\mathbf{v} = \mathbf{u}_h$  in (3.5a) and  $q = p_h$  in (3.5b) and add the two equations, then we obtain

$$\mathbf{a}_w(\mathbf{u}_h, \mathbf{u}_h) = 0.$$

Thus, it follows from (4.4) that  $\|\mathbf{u}_h\| = 0$ , so  $\mathbf{u}_h = \mathbf{0}$ . Moreover, the fact  $\mathbf{u}_h = \mathbf{0}$  in (3.5) implies

$$\mathbf{b}_w(\mathbf{v}, p_h) = 0, \quad \forall \mathbf{v} \in \mathbf{V}_h.$$

Therefore, we have  $\|p_h\|_0 = 0$  from (4.2), which gives  $p_h = 0$ . □

## 4.2 Error estimates

We prove error estimates for velocity and pressure with respect to the mesh-dependent norm  $\|\cdot\|$  and the  $L^2$ -norm, respectively. Let  $\Pi_h : [H^2(\Omega)]^d \rightarrow \mathbf{V}_h$  be the interpolation operator [34] such that

$$\Pi_h \mathbf{v} = \Pi_h^C \mathbf{v} + \Pi_h^D \mathbf{v},$$

where  $\Pi_h^C \mathbf{v} \in \mathbf{C}_h$  is the nodal value interpolant of  $\mathbf{v}$  and  $\Pi_h^D \mathbf{v} \in \mathbf{D}_h$  satisfies  $(\nabla \cdot \Pi_h^D \mathbf{v}, 1)_T = (\nabla \cdot (\mathbf{v} - \Pi_h^C \mathbf{v}), 1)_T$  for all  $T \in \mathcal{T}_h$ . The corresponding interpolation error estimates [34] are as follows:

$$|\mathbf{v} - \Pi_h \mathbf{v}|_{j, \mathcal{T}_h} \leq Ch^{m-j} |\mathbf{v}|_m, \quad 0 \leq j \leq m \leq 2, \quad \forall \mathbf{v} \in [H^2(\Omega)]^d, \quad (4.6a)$$

$$\|\mathbf{v} - \Pi_h \mathbf{v}\|_{\mathcal{E}} \leq Ch \|\mathbf{v}\|_2, \quad \forall \mathbf{v} \in [H^2(\Omega)]^d. \quad (4.6b)$$

We also introduce the local  $L^2$ -projection  $\mathcal{P}_0 : H^1(\Omega) \rightarrow Q_h$  satisfying  $(q - \mathcal{P}_0 q, 1)_T = 0$  for all  $T \in \mathcal{T}_h$  and its error estimate,

$$\|q - \mathcal{P}_0 q\|_0 \leq Ch \|q\|_1, \quad \forall q \in H^1(\Omega). \quad (4.7)$$

Furthermore, let us denote  $\Theta_h : [H^2(\Omega)]^d \rightarrow \mathbf{V}_h$  as

$$\Theta_h \mathbf{u} = \{\Theta_0 \mathbf{u}, \Theta_b \mathbf{u}\},$$

where  $\Theta_0$  and  $\Theta_b$  are the local  $L^2$ -projections onto  $[P_1(T)]^d$  for all  $T \in \mathcal{T}_h$  and  $[P_1(e)]^d$  for all  $e \in \mathcal{E}_h$ , respectively. Then, we have the following commutative property [30],

$$\nabla_w(\Theta_h \mathbf{v}) = \Theta_h(\nabla \mathbf{v}), \quad (4.8)$$

where  $\Theta_h$  is the local  $L^2$ -projection onto  $[P_0(T)]^{d \times d}$ .

We define error functions used in the error estimates,

$$\chi_h = \mathbf{u} - \Pi_h \mathbf{u}, \quad \mathbf{e}_h = \Pi_h \mathbf{u} - \mathbf{u}_h, \quad \xi_h = p - \mathcal{P}_0 p, \quad \epsilon_h = \mathcal{P}_0 p - p_h. \quad (4.9)$$

Then, we derive the main error equations in the following lemma.

**Lemma 4.6.** For any  $\mathbf{v} \in \mathbf{V}_h$  and  $q \in Q_h$ , we have

$$\mathbf{a}_w(\mathbf{e}_h, \mathbf{v}) - \mathbf{b}_w(\mathbf{v}, \epsilon_h) = l_1(\mathbf{u}, \mathbf{v}) + l_2(\mathbf{u}, \mathbf{v}) + \mathbf{s}(\Pi_h \mathbf{u}, \mathbf{v}) + \mathbf{b}_w(\mathbf{v}, \xi_h), \quad (4.10a)$$

$$\mathbf{b}_w(\mathbf{e}_h, q) = -\mathbf{b}_w(\chi_h, q), \quad (4.10b)$$

where the supplemental bilinear forms are defined as follows:

$$l_1(\mathbf{u}, \mathbf{v}) = \nu \sum_{T \in \mathcal{T}_h} \langle \nabla \mathbf{u} \cdot \mathbf{n} - \Theta_h(\nabla \mathbf{u}) \cdot \mathbf{n}, \mathbf{v} - \{\mathbf{v}\} \rangle_{\partial T},$$

$$l_2(\mathbf{u}, \mathbf{v}) = \nu (\nabla_w(\Pi_h \mathbf{u} - \Theta_h \mathbf{u}), \nabla_w \mathbf{v})_{\mathcal{T}_h},$$

$$\mathbf{s}(\Pi_h \mathbf{u}, \mathbf{v}) = \nu \langle h_e^{-1}[\Pi_h \mathbf{u}], [\mathbf{v}] \rangle_{\mathcal{E}_h}.$$

*Proof.* For any  $\mathbf{v} \in \mathbf{V}_h$ , integration by parts and the definition of  $\Theta_h$  imply

$$\begin{aligned} (-\Delta \mathbf{u}, \mathbf{v})_{\mathcal{T}_h} &= - \sum_{T \in \mathcal{T}_h} \langle \nabla \mathbf{u} \cdot \mathbf{n}, \mathbf{v} \rangle_{\partial T} + (\nabla \mathbf{u}, \nabla \mathbf{v})_{\mathcal{T}_h} \\ &= - \sum_{T \in \mathcal{T}_h} \langle \nabla \mathbf{u} \cdot \mathbf{n}, \mathbf{v} - \{\mathbf{v}\} \rangle_{\partial T} + (\Theta_h(\nabla \mathbf{u}), \nabla \mathbf{v})_{\mathcal{T}_h}. \end{aligned}$$

Then, the definition of the weak gradient and the commutative property (4.8) lead to

$$\begin{aligned} (\Theta_h(\nabla \mathbf{u}), \nabla \mathbf{v})_{\mathcal{T}_h} &= (\Theta_h(\nabla \mathbf{u}), \nabla_w \mathbf{v})_{\mathcal{T}_h} + (\Theta_h(\nabla \mathbf{u}), \nabla \mathbf{v} - \nabla_w \mathbf{v})_{\mathcal{T}_h} \\ &= (\nabla_w(\Theta_h \mathbf{u}), \nabla_w \mathbf{v})_{\mathcal{T}_h} + \sum_{T \in \mathcal{T}_h} \langle \Theta_h(\nabla \mathbf{u}) \cdot \mathbf{n}, \mathbf{v} - \{\mathbf{v}\} \rangle_{\partial T}. \end{aligned}$$

Hence, we obtain

$$\begin{aligned} (-\Delta \mathbf{u}, \mathbf{v})_{\mathcal{T}_h} &= (\nabla_w(\Theta_h \mathbf{u}), \nabla_w \mathbf{v})_{\mathcal{T}_h} - \sum_{T \in \mathcal{T}_h} \langle \nabla \mathbf{u} \cdot \mathbf{n} - \Theta_h(\nabla \mathbf{u}) \cdot \mathbf{n}, \mathbf{v} - \{\mathbf{v}\} \rangle_{\partial T}, \\ (\nabla p, \mathbf{v})_{\mathcal{T}_h} &= \mathbf{b}_w(\mathbf{v}, p), \end{aligned}$$

where the second equation is obtained by the trace identity (2.1), the continuity of  $p$ , and (3.4b). Then, by combining the above two equations in the equation (1.1a), we have

$$(\nabla_w(\Theta_h \mathbf{u}), \nabla_w \mathbf{v})_{\mathcal{T}_h} - \mathbf{b}_w(\mathbf{v}, p) = (\mathbf{f}, \mathbf{v}) + l_1(\mathbf{u}, \mathbf{v}).$$

If we add proper terms including  $\Pi_h \mathbf{u}$  to both sides and subtract  $\mathbf{b}_w(\mathbf{v}, P_0 p)$  from both sides, we get

$$\mathbf{a}_w(\Pi_h \mathbf{u}, \mathbf{v}) - \mathbf{b}_w(\mathbf{v}, P_0 p) = (\mathbf{f}, \mathbf{v}) + l_1(\mathbf{u}, \mathbf{v}) + l_2(\mathbf{u}, \mathbf{v}) + \mathbf{s}(\Pi_h \mathbf{u}, \mathbf{v}) + \mathbf{b}_w(\mathbf{v}, \xi_h).$$

By comparing this equation with (3.5a) in the mEG method, we arrive at

$$\mathbf{a}_w(\mathbf{e}_h, \mathbf{v}) - \mathbf{b}_w(\mathbf{v}, \epsilon_h) = l_1(\mathbf{u}, \mathbf{v}) + l_2(\mathbf{u}, \mathbf{v}) + \mathbf{s}(\Pi_h \mathbf{u}, \mathbf{v}) + \mathbf{b}_w(\mathbf{v}, \xi_h).$$

Furthermore, the continuity of  $\mathbf{u}$  and (3.5b) imply

$$(\nabla \cdot \mathbf{u}, q)_{\mathcal{T}_h} = \mathbf{b}_w(\mathbf{u}, q) = 0 = \mathbf{b}_w(\mathbf{u}_h, q),$$

so (4.10b) is obtained by subtracting  $\mathbf{b}_w(\Pi_h \mathbf{u}, q)$  from both sides.  $\square$

We provide the upper bounds for the supplementary bilinear forms in Lemma 4.6.

**Lemma 4.7.** We assume that  $\mathbf{w} \in [H^2(\Omega)]^d$  and  $\mathbf{v} \in \mathbf{V}_h$ . Then, we have

$$|l_1(\mathbf{w}, \mathbf{v})| \leq C\nu h \|\mathbf{w}\|_2 \|\mathbf{v}\|, \quad (4.11a)$$

$$|l_2(\mathbf{w}, \mathbf{v})| \leq C\nu h \|\mathbf{w}\|_2 \|\mathbf{v}\|, \quad (4.11b)$$

$$|\mathbf{s}(\Pi_h \mathbf{w}, \mathbf{v})| \leq C\nu h \|\mathbf{w}\|_2 \|\mathbf{v}\|, \quad (4.11c)$$

where the constant  $C$  is independent of  $h$ .



*Proof.* The proof of the bound (4.11a) can be found in [24], so we focus on showing (4.11b) and (4.11c) here. The definition of the weak gradient and the properties of the projections  $\Pi_h$  and  $\Theta_h$  lead to

$$\begin{aligned}
|l_2(\mathbf{w}, \mathbf{v})| &= \nu \left| (\nabla_w(\Pi_h \mathbf{w} - \Theta_h \mathbf{w}), \nabla_w \mathbf{v}) \right|_{\mathcal{T}_h} \\
&= \nu \left| \sum_{T \in \mathcal{T}_h} \langle \{\Pi_h \mathbf{w}\} - \Theta_h \mathbf{w}, \nabla_w \mathbf{v} \cdot \mathbf{n} \rangle_{\partial T} \right| \\
&= \nu \left| \sum_{T \in \mathcal{T}_h} \langle \{\Pi_h \mathbf{w} - \mathbf{w}\}, \nabla_w \mathbf{v} \cdot \mathbf{n} \rangle_{\partial T} \right| \\
&\leq \nu \sum_{T \in \mathcal{T}_h} \|h_T^{-1/2} \{\Pi_h \mathbf{w} - \mathbf{w}\}\|_{\partial T} \|h_T^{1/2} \nabla_w \mathbf{v}\|_{\partial T} \\
&\leq C\nu h \|\mathbf{w}\|_2 \|\nabla_w \mathbf{v}\|_{0, \mathcal{T}_h}
\end{aligned}$$

The third identity holds true because  $\mathbf{w} \in [H^2(\Omega)]^d$  is continuous on  $\partial T$ , and the last inequality is obtained from the trace inequality (2.2) and (4.6a).

For the stabilization term (4.11c), it follows from the Cauchy-Schwarz inequality, (2.2), and (4.6a) that

$$\begin{aligned}
|\mathbf{s}(\Pi_h \mathbf{w}, \mathbf{v})| &= \nu \left| \langle h_e^{-1} [\Pi_h \mathbf{w} - \mathbf{w}], [\mathbf{v}] \rangle_{\mathcal{E}_h} \right| \\
&\leq C\nu \|h_e^{-1/2} [\Pi_h \mathbf{w} - \mathbf{w}]\|_{0, \mathcal{E}_h} \|h_e^{-1/2} [\mathbf{v}]\|_{0, \mathcal{E}_h} \\
&\leq C\nu h \|\mathbf{w}\|_2 \|\mathbf{v}\|.
\end{aligned}$$

□

Consequently, we obtain the following error estimates.

**Theorem 4.8.** *Let  $(\mathbf{u}, p) \in [H_0^1(\Omega) \cap H^2(\Omega)]^d \times (L_0^2(\Omega) \cap H^1(\Omega))$  be the solution to (1.1a)-(1.1c), and  $(\mathbf{u}_h, p_h) \in \mathbf{V}_h \times Q_h$  be the discrete solution from the mEG method. Then, we have the following error estimates*

$$\begin{aligned}
\|\Pi_h \mathbf{u} - \mathbf{u}_h\| &\leq Ch \left( \|\mathbf{u}\|_2 + \frac{1}{\nu} \|p\|_1 \right), \\
\|\mathcal{P}_0 p - p_h\|_0 &\leq Ch (\nu \|\mathbf{u}\|_2 + \|p\|_1).
\end{aligned}$$

*Proof.* First, we see the error equation (4.10a), for any  $\mathbf{v} \in \mathbf{V}_h$  and  $q \in Q_h$ ,

$$\mathbf{b}_w(\mathbf{v}, \epsilon_h) = \mathbf{a}_w(\mathbf{e}_h, \mathbf{v}) - l_1(\mathbf{u}, \mathbf{v}) - l_2(\mathbf{u}, \mathbf{v}) - \mathbf{s}(\Pi_h \mathbf{u}, \mathbf{v}) - \mathbf{b}_w(\mathbf{v}, \xi_h).$$

Then, it follows from (4.5), (4.11), (4.3), and (4.7) that

$$\begin{aligned}
|\mathbf{b}_w(\mathbf{v}, \epsilon_h)| &\leq C (\nu \|\mathbf{e}_h\| \|\mathbf{v}\| + \nu h \|\mathbf{u}\|_2 \|\mathbf{v}\| + \|\xi_h\|_0 \|\mathbf{v}\|) \\
&\leq C (\nu \|\mathbf{e}_h\| + \nu h \|\mathbf{u}\|_2 + h \|p\|_1) \|\mathbf{v}\|.
\end{aligned}$$

The inf-sup condition (4.2) implies that

$$\|\epsilon_h\|_0 \leq C (\nu \|\mathbf{e}_h\| + h (\nu \|\mathbf{u}\|_2 + \|p\|_1)). \quad (4.12)$$

Moreover, by choosing  $\mathbf{v} = \mathbf{e}_h$  and  $q = \epsilon_h$  in (4.10) and substituting (4.10b) into (4.10a), we obtain

$$\mathbf{a}_w(\mathbf{e}_h, \mathbf{e}_h) = -\mathbf{b}_w(\boldsymbol{\chi}_h, \epsilon_h) + l_1(\mathbf{u}, \mathbf{e}_h) + l_2(\mathbf{u}, \mathbf{e}_h) + \mathbf{s}(\Pi_h \mathbf{u}, \mathbf{e}_h) + \mathbf{b}_w(\mathbf{e}_h, \xi_h).$$

Here, we show an upper bound for the term  $\mathbf{b}_w(\boldsymbol{\chi}_h, \epsilon_h)$ . Integration by parts and the trace identity (2.1) give

$$\begin{aligned}
\mathbf{b}_w(\boldsymbol{\chi}_h, \epsilon_h) &= \mathbf{b}(\boldsymbol{\chi}_h, \epsilon_h) \\
&= (\nabla \cdot \boldsymbol{\chi}_h, \epsilon_h)_{\mathcal{T}_h} - \langle [\boldsymbol{\chi}_h] \cdot \mathbf{n}_e, \{\epsilon_h\} \rangle_{\mathcal{E}_h} \\
&= \sum_{T \in \mathcal{T}_h} \langle \boldsymbol{\chi}_h \cdot \mathbf{n}, \epsilon_h \rangle_{\partial T} - \langle [\boldsymbol{\chi}_h] \cdot \mathbf{n}_e, \{\epsilon_h\} \rangle_{\mathcal{E}_h} \\
&= \langle \{\boldsymbol{\chi}_h\} \cdot \mathbf{n}_e, [\epsilon_h] \rangle_{\mathcal{E}_h^o}.
\end{aligned}$$

Thus, it follows from the Cauchy-Schwarz inequality, (2.2), and (4.6a) that

$$|\mathbf{b}_w(\boldsymbol{\chi}_h, \boldsymbol{\epsilon}_h)| \leq \| \{\boldsymbol{\chi}_h\} \|_{0, \mathcal{E}_h} \| \boldsymbol{\epsilon}_h \|_{0, \mathcal{E}_h} \leq Ch \| \mathbf{u} \|_2 \| \boldsymbol{\epsilon}_h \|_0. \quad (4.13)$$

Hence, by (4.4), (4.11), (4.3), (4.7), (4.12), and (4.13), we have

$$\nu \| \mathbf{e}_h \|_2^2 \leq C (\nu h \| \mathbf{u} \|_2 \| \mathbf{e}_h \| + h \| p \|_1 \| \mathbf{e}_h \| + \nu h^2 \| \mathbf{u} \|_2^2 + h^2 \| \mathbf{u} \|_2 \| p \|_1).$$

We also apply the Young's inequality with a positive constant  $\kappa$  satisfying  $\kappa < 1/C$ ,

$$\begin{aligned} \nu h \| \mathbf{u} \|_2 \| \mathbf{e}_h \| &\leq \nu \left( \frac{h^2}{2\kappa} \| \mathbf{u} \|_2^2 + \frac{\kappa}{2} \| \mathbf{e}_h \|_2^2 \right), \\ h \| p \|_1 \| \mathbf{e}_h \| &\leq \left( \frac{h^2}{2\nu\kappa} \| p \|_1^2 + \frac{\nu\kappa}{2} \| \mathbf{e}_h \|_2^2 \right), \\ h^2 \| \mathbf{u} \|_2 \| p \|_1 &\leq \left( \frac{\nu h^2}{2} \| \mathbf{u} \|_2^2 + \frac{h^2}{2\nu} \| p \|_1^2 \right). \end{aligned}$$

We finally obtain

$$\nu \| \mathbf{e}_h \|_2^2 \leq C \left( \nu h^2 \| \mathbf{u} \|_2^2 + \frac{h^2}{\nu} \| p \|_1^2 \right),$$

which implies that

$$\| \mathbf{e}_h \| \leq Ch \left( \| \mathbf{u} \|_2 + \frac{1}{\nu} \| p \|_1 \right).$$

In addition, together with this velocity error estimate, the estimate (4.12) implies

$$\| \boldsymbol{\epsilon}_h \|_0 \leq Ch (\nu \| \mathbf{u} \|_2 + \| p \|_1).$$

□

Finally, we present the total error estimates showing the optimal rates of convergence in both velocity and pressure.

**Theorem 4.9.** *Under the same assumption of Theorem 4.8, we have the following error estimates*

$$\begin{aligned} \| \mathbf{u} - \mathbf{u}_h \| &\leq Ch \left( \| \mathbf{u} \|_2 + \frac{1}{\nu} \| p \|_1 \right), \\ \| p - p_h \|_0 &\leq Ch (\nu \| \mathbf{u} \|_2 + \| p \|_1). \end{aligned}$$

*Proof.* The estimates in this theorem are readily proved by the triangle inequality, the interpolation error estimates (4.6b) and (4.7), and the norm equivalence (4.1). □

## 5 A Pressure-Robust Modified Enriched Galerkin Method

In this section, we derive a pressure-robust scheme associated with the mEG method (Algorithm 2) by applying the velocity reconstruction operator [17] to the load vector on the right hand side. The operator  $\mathcal{R} : \mathbf{V}_h \rightarrow \mathcal{BDM}_1(\mathcal{T}_h) \subset H(\text{div}, \Omega)$  is defined by

$$\int_e (\mathcal{R}\mathbf{v}) \cdot \mathbf{n}_e p_1 \, ds = \int_e \{\mathbf{v}\} \cdot \mathbf{n}_e p_1 \, ds, \quad \forall p_1 \in P_1(e), \forall e \in \mathcal{E}_h^e, \quad (5.1a)$$

$$\int_e (\mathcal{R}\mathbf{v}) \cdot \mathbf{n}_e p_1 \, ds = 0, \quad \forall p_1 \in P_1(e), \forall e \in \mathcal{E}_h^b, \quad (5.1b)$$

when  $\mathcal{BDM}_1(\mathcal{T}_h)$  denotes the Brezzi-Douglas-Marini space of index 1 on  $\mathcal{T}_h$ .

---

**Algorithm 3** Pressure-robust modified enriched Galerkin (PR-mEG) method

---

Find  $(\mathbf{u}_h, p_h) \in \mathbf{V}_h \times Q_h$  such that

$$\mathbf{a}_w(\mathbf{u}_h, \mathbf{v}) - \mathbf{b}_w(\mathbf{v}, p_h) = (\mathbf{f}, \mathcal{R}\mathbf{v})_{\mathcal{T}_h}, \quad \forall \mathbf{v} \in \mathbf{V}_h, \quad (5.2a)$$

$$\mathbf{b}_w(\mathbf{u}_h, q) = 0, \quad \forall q \in Q_h, \quad (5.2b)$$

where  $\mathbf{a}_w(\cdot, \cdot)$  and  $\mathbf{b}_w(\cdot, \cdot)$  are the same as (3.6a) and (3.6b), respectively.

---

**Remark 5.1.** The **mEG** method in Algorithm 2 and **PR-mEG** method in Algorithm 3 have the same formulation on left hand side that consists of  $\mathbf{a}_w(\cdot, \cdot)$  and  $\mathbf{b}_w(\cdot, \cdot)$ . The only difference is that a reconstructed test function is applied to the load vector on the right hand side. This implies that the well-posedness of the **PR-mEG** method is guaranteed by that of the **mEG** method, and moreover, both of the **mEG** and **PR-mEG** methods produce the same stiffness matrix.

The error equations corresponding to the **PR-mEG** method are derived in the following lemma using the same error functions in (4.9).

**Lemma 5.2.** *For any  $\mathbf{v} \in \mathbf{V}_h$  and  $q \in Q_h$ , we have*

$$\mathbf{a}_w(\mathbf{e}_h, \mathbf{v}) - \mathbf{b}_w(\mathbf{v}, \epsilon_h) = l_1(\mathbf{u}, \mathbf{v}) + l_2(\mathbf{u}, \mathbf{v}) + l_3(\mathbf{u}, \mathbf{v}) + \mathbf{s}(\Pi_h \mathbf{u}, \mathbf{v}), \quad (5.3a)$$

$$\mathbf{b}_w(\mathbf{e}_h, q) = -\mathbf{b}_w(\chi_h, q), \quad (5.3b)$$

where  $l_1(\cdot, \cdot)$ ,  $l_2(\cdot, \cdot)$ , and  $\mathbf{s}(\cdot, \cdot)$  are defined in Lemma 4.6, and another supplemental bilinear form is defined by

$$l_3(\mathbf{u}, \mathbf{v}) = -\nu (\Delta \mathbf{u}, \mathbf{v} - \mathcal{R}\mathbf{v})_{\mathcal{T}_h}$$

*Proof.* First of all, we obtain the following identities,

$$(\nabla p, \mathcal{R}\mathbf{v})_{\mathcal{T}_h} = -\mathbf{b}(\mathbf{v}, \mathcal{P}_0 p) = -\mathbf{b}_w(\mathbf{v}, \mathcal{P}_0 p)$$

because  $\mathcal{R}\mathbf{v} \cdot \mathbf{n}$  is continuous on  $\partial T$  and  $\nabla \cdot \mathcal{R}\mathbf{v}$  is constant in  $T$ . (See [17] for details.) Moreover, we have

$$(-\Delta \mathbf{u}, \mathcal{R}\mathbf{v})_{\mathcal{T}_h} = (-\Delta \mathbf{u}, \mathbf{v})_{\mathcal{T}_h} + (\Delta \mathbf{u}, \mathbf{v} - \mathcal{R}\mathbf{v})_{\mathcal{T}_h}.$$

Then, it follows from (1.1a) and the error equations in Lemma 4.6 that

$$\mathbf{a}_w(\Pi_h \mathbf{u}, \mathbf{v}) - \mathbf{b}_w(\mathbf{v}, \mathcal{P}_0 p) = (\mathbf{f}, \mathcal{R}\mathbf{v})_{\mathcal{T}_h} + l_1(\mathbf{u}, \mathbf{v}) + l_2(\mathbf{u}, \mathbf{v}) + l_3(\mathbf{u}, \mathbf{v}) + \mathbf{s}(\Pi_h \mathbf{u}, \mathbf{v}).$$

By subtracting (5.2a) from this equation, we arrive at the equation (5.3a). The equation (5.3b) is simply derived in the same way as Lemma 4.6.  $\square$

Consequently, the following theorem theoretically shows pressure-robustness of the **PR-mEG** method.

**Theorem 5.3.** *Let  $(\mathbf{u}, p) \in [H_0^1(\Omega) \cap H^2(\Omega)]^d \times (L_0^2(\Omega) \cap H^1(\Omega))$  be the solution to (1.1a)-(1.1c), and  $(\mathbf{u}_h, p_h) \in \mathbf{V}_h \times Q_h$  be the discrete solution from the **PR-mEG** method. Then, we have the following error estimates*

$$\|\Pi_h \mathbf{u} - \mathbf{u}_h\| \leq Ch \|\mathbf{u}\|_2, \quad \|\mathcal{P}_0 p - p_h\|_0 \leq C\nu h \|\mathbf{u}\|_2.$$

Therefore, the total error estimates are as follows:

$$\|\mathbf{u} - \mathbf{u}_h\| \leq Ch \|\mathbf{u}\|_2, \quad \|p - p_h\|_0 \leq Ch (\nu \|\mathbf{u}\|_2 + \|p\|_1).$$

*Proof.* To begin with, we observe the error equation (5.3a),

$$\mathbf{b}_w(\mathbf{v}, \epsilon_h) = \mathbf{a}_w(\mathbf{e}_h, \mathbf{v}) - l_1(\mathbf{u}, \mathbf{v}) - l_2(\mathbf{u}, \mathbf{v}) - l_3(\mathbf{u}, \mathbf{v}) - \mathbf{s}(\Pi_h \mathbf{u}, \mathbf{v}).$$

Here, the bilinear form  $l_3(\mathbf{u}, \mathbf{v})$  is bounded using the Cauchy-Schwarz inequality,

$$|l_3(\mathbf{u}, \mathbf{v})| \leq \nu \|\Delta \mathbf{u}\|_0 \|\mathbf{v} - \mathcal{R}\mathbf{v}\|_0 \leq \nu \|\mathbf{u}\|_2 \|\mathbf{v} - \mathcal{R}\mathbf{v}\|_0.$$

It also follows from the estimate  $\|\mathbf{v} - \mathcal{R}\mathbf{v}\|_0$  in [17] and the norm equivalence (4.1) that

$$\|\mathbf{v} - \mathcal{R}\mathbf{v}\|_0 \leq Ch \|\mathbf{v}\|,$$

so we arrive at

$$|l_3(\mathbf{u}, \mathbf{v})| \leq C\nu h \|\mathbf{u}\|_2 \|\mathbf{v}\|. \quad (5.4)$$

Thus, from (4.5), (4.11), and (5.4), we obtain

$$|\mathbf{b}_w(\mathbf{v}, \epsilon_h)| \leq C (\nu \|\mathbf{e}_h\| + \nu h \|\mathbf{u}\|_2) \|\mathbf{v}\|.$$

Hence, the inf-sup condition (4.2) leads to

$$\|\epsilon_h\|_0 \leq C\nu (\|\mathbf{e}_h\| + h \|\mathbf{u}\|_2). \quad (5.5)$$

Similar to the proof of Theorem 4.8, choosing  $\mathbf{v} = \mathbf{e}_h$  and  $q = \epsilon_h$  yields that

$$\mathbf{a}_w(\mathbf{e}_h, \mathbf{e}_h) = -\mathbf{b}_w(\boldsymbol{\chi}_h, \epsilon_h) + l_1(\mathbf{u}, \mathbf{e}_h) + l_2(\mathbf{u}, \mathbf{e}_h) + l_3(\mathbf{u}, \mathbf{e}_h) + \mathbf{s}(\Pi_h \mathbf{u}, \mathbf{e}_h).$$

From (4.13) and (5.5), we get the following intermediate result,

$$|\mathbf{b}_w(\boldsymbol{\chi}_h, \epsilon_h)| \leq Ch\|\mathbf{u}\|_2\|\epsilon_h\|_0 \leq C\nu h\|\mathbf{u}\|_2 (\|\mathbf{e}_h\| + h\|\mathbf{u}\|_2).$$

Therefore, it follows from (4.4), (4.11), and (5.4) that

$$\nu\|\mathbf{e}_h\|^2 \leq C\nu (h\|\mathbf{u}\|_2\|\mathbf{e}_h\| + h^2\|\mathbf{u}\|_2^2).$$

The Young's inequality gives

$$h\|\mathbf{u}\|_2\|\mathbf{e}_h\| \leq \frac{h^2}{2\kappa}\|\mathbf{u}\|_2^2 + \frac{\kappa}{2}\|\mathbf{e}_h\|^2,$$

so choosing a proper  $\kappa$  implies

$$\nu\|\mathbf{e}_h\|^2 \leq C\nu h^2\|\mathbf{u}\|_2^2.$$

Therefore, together with (5.5), we obtain

$$\|\mathbf{e}_h\| \leq Ch\|\mathbf{u}\|_2, \quad \|\epsilon_h\|_0 \leq C\nu h\|\mathbf{u}\|_2.$$

□

## 6 Numerical Experiments

In this section, we present numerical experiments validating our theoretical results with two- and three-dimensional examples. The numerical experiments are implemented by authors' codes developed based on iFEM [9]. The numerical methods mentioned in this paper and their discrete solutions are denoted as follows:

- $(\mathbf{u}_h^{\text{EG}}, p_h^{\text{EG}})$ : Solution by the EG method [33] in Algorithm 1.
- $(\mathbf{u}_h^{\text{mEG}}, p_h^{\text{mEG}})$ : Solution by the mEG method in Algorithm 2.
- $(\mathbf{u}_h^{\text{PR}}, p_h^{\text{PR}})$ : Solution by the PR-mEG method in Algorithm 3.

We compare the penalty terms in the EG and mEG methods,

$$\text{EG : Penalty term of } \mathbf{a}(\mathbf{u}_h^{\text{EG}}, \mathbf{v}) \rightarrow \nu\rho\langle h_e^{-1}[\mathbf{u}_h^{\text{EG}}], [\mathbf{v}] \rangle_{\mathcal{E}_h}, \quad (6.1)$$

$$\text{mEG : Penalty term of } \mathbf{a}_w(\mathbf{u}_h^{\text{mEG}}, \mathbf{v}) \rightarrow \nu\rho_m\langle h_e^{-1}[\mathbf{u}_h^{\text{mEG}}], [\mathbf{v}] \rangle_{\mathcal{E}_h}, \quad (6.2)$$

where  $\rho_m$  is a hypothetical mEG penalty parameter for comparison and the mEG method uses the fixed parameter  $\rho_m = 1$ . While a sufficiently large penalty parameter  $\rho$  is required for the EG method, our mEG method ( $\rho_m = 1$ ) is a parameter-free EG method under the same finite dimensional velocity and pressure spaces. We recall the error estimates for the mEG method in Section 4:

$$\|\|\Pi_h \mathbf{u} - \mathbf{u}_h^{\text{mEG}}\|\| \lesssim h (\|\mathbf{u}\|_2 + \nu^{-1}\|p\|_1), \quad \|\mathcal{P}_0 p - p_h^{\text{mEG}}\|_0 \lesssim h (\nu\|\mathbf{u}\|_2 + \|p\|_1), \quad (6.3a)$$

$$\|\|\mathbf{u} - \mathbf{u}_h^{\text{mEG}}\|\| \lesssim h (\|\mathbf{u}\|_2 + \nu^{-1}\|p\|_1), \quad \|p - p_h^{\text{mEG}}\|_0 \lesssim h (\nu\|\mathbf{u}\|_2 + \|p\|_1), \quad (6.3b)$$

which means the same rates of convergence as the EG method. Moreover, we developed a pressure-robust numerical scheme corresponding to the mEG method, and the error estimates for the PR-mEG method proved in Section 5 are as follows:

$$\|\|\Pi_h \mathbf{u} - \mathbf{u}_h^{\text{PR}}\|\| \lesssim h\|\mathbf{u}\|_2, \quad \|\mathcal{P}_0 p - p_h^{\text{PR}}\|_0 \lesssim \nu h\|\mathbf{u}\|_2, \quad (6.4a)$$

$$\|\|\mathbf{u} - \mathbf{u}_h^{\text{PR}}\|\| \lesssim h\|\mathbf{u}\|_2, \quad \|p - p_h^{\text{PR}}\|_0 \lesssim h (\nu\|\mathbf{u}\|_2 + \|p\|_1). \quad (6.4b)$$

In two- and three-dimensional examples, we demonstrate the well-posedness and optimal rates of convergence for the mEG method. By checking the behaviors of the errors with decreasing viscosity  $\nu$ , we confirm the error estimates of the PR-mEG method in (6.4), which means more accurate numerical solutions than the mEG method in the case of small viscosity  $\nu \ll 1$ .

## 6.1 Two dimensional examples

Let the computational domain be  $\Omega = (0, 1) \times (0, 1)$ . The velocity field and pressure are chosen as

$$\mathbf{u} = \begin{pmatrix} 10x^2(x-1)^2y(y-1)(2y-1) \\ -10x(x-1)(2x-1)y^2(y-1)^2 \end{pmatrix}, \quad p = 10(2x-1)(2y-1). \quad (6.5)$$

Then, the body force  $\mathbf{f}$  is obtained from the Stokes equations in (1.1), and the homogeneous boundary condition for velocity is considered.

### 6.1.1 Parameter-free test

We check the errors and condition numbers of the stiffness matrices for the EG and mEG methods with different penalty parameters. To see how the penalty parameters affect the performance of the two methods, we apply the penalty terms (6.1)-(6.2) and change  $\rho$  and  $\rho_m$  from 0.1 to 5. In the test, we choose the uniform triangular mesh with  $h = 1/16$  and the viscosity  $\nu = 1$ . Figure 1 shows that the

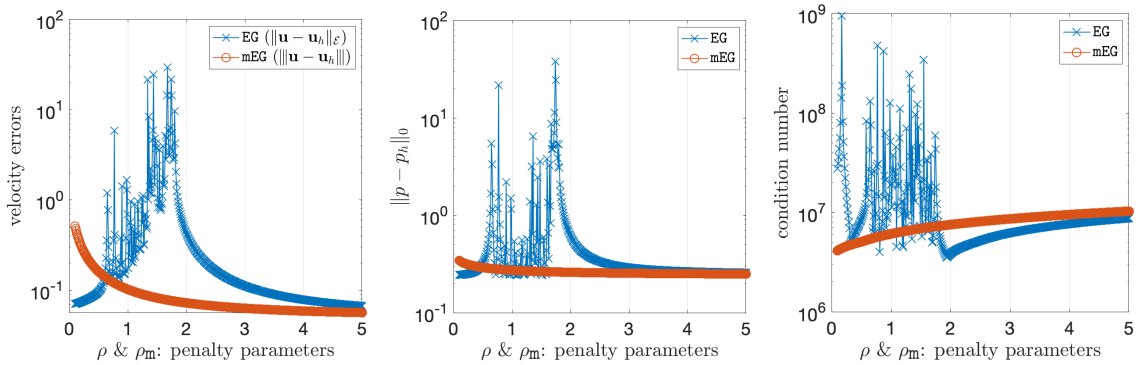


Figure 1: Errors and condition numbers of EG and mEG for  $0.1 \leq \rho, \rho_m \leq 5$  ( $\nu = 1$ ,  $h = 1/16$ ).

EG method seems to yield unstable errors and condition numbers with penalty parameters less than 2, which implies the need of a sufficiently large parameter for the stability. On the other hand, the mEG method shows stable behaviors in the errors and condition numbers for any positive parameter  $\rho_m$ .

$h$	EG ( $\rho = 1$ )		mEG ( $\rho_m = 1$ )	
	$\ \mathbf{u} - \mathbf{u}_h^{\text{EG}}\ _{\mathcal{E}}$	Rate	$\ \mathbf{u} - \mathbf{u}_h^{\text{mEG}}\ $	Rate
1/8	7.394e-1	-	2.749e-1	-
1/16	6.931e-1	0.09	1.024e-1	1.42
1/32	2.440e-1	1.51	3.940e-2	1.38
1/64	9.052e-2	1.43	1.606e-2	1.29
$h$	$\ p - p_h^{\text{EG}}\ _0$	Rate	$\ p - p_h^{\text{mEG}}\ _0$	Rate
1/8	9.299e-1	-	5.815e-1	-
1/16	2.897e-1	1.68	2.733e-1	1.09
1/32	2.319e-1	0.32	1.322e-1	1.05
1/64	2.664e-1	-0.20	6.498e-2	1.02

Table 1: A mesh refinement study for EG and mEG with varying mesh size  $h$  and  $\nu = 1$ .

We also perform a mesh refinement study for the EG and mEG methods when  $\rho = \rho_m = 1$ . In Table 1, the errors of the EG method fail to converge due to the insufficiently large penalty parameter. However, the mEG method produces the velocity and pressure errors that indicate at least the first-order convergence.

Moreover, we compare the numerical solutions of the EG and mEG methods when  $h = 1/16$ ,  $\nu = 1$ , and  $\rho = \rho_m = 1$ . In Figure 2, the numerical velocity of the EG method roughly captures the vortex flow pattern, but some relatively large jumps appear throughout the numerical velocity solution. The mEG method, however, produces more stable numerical velocity that well captures the pattern compared to the EG method.

We also conduct the parameter-free test on various meshes presented in Figure 3:

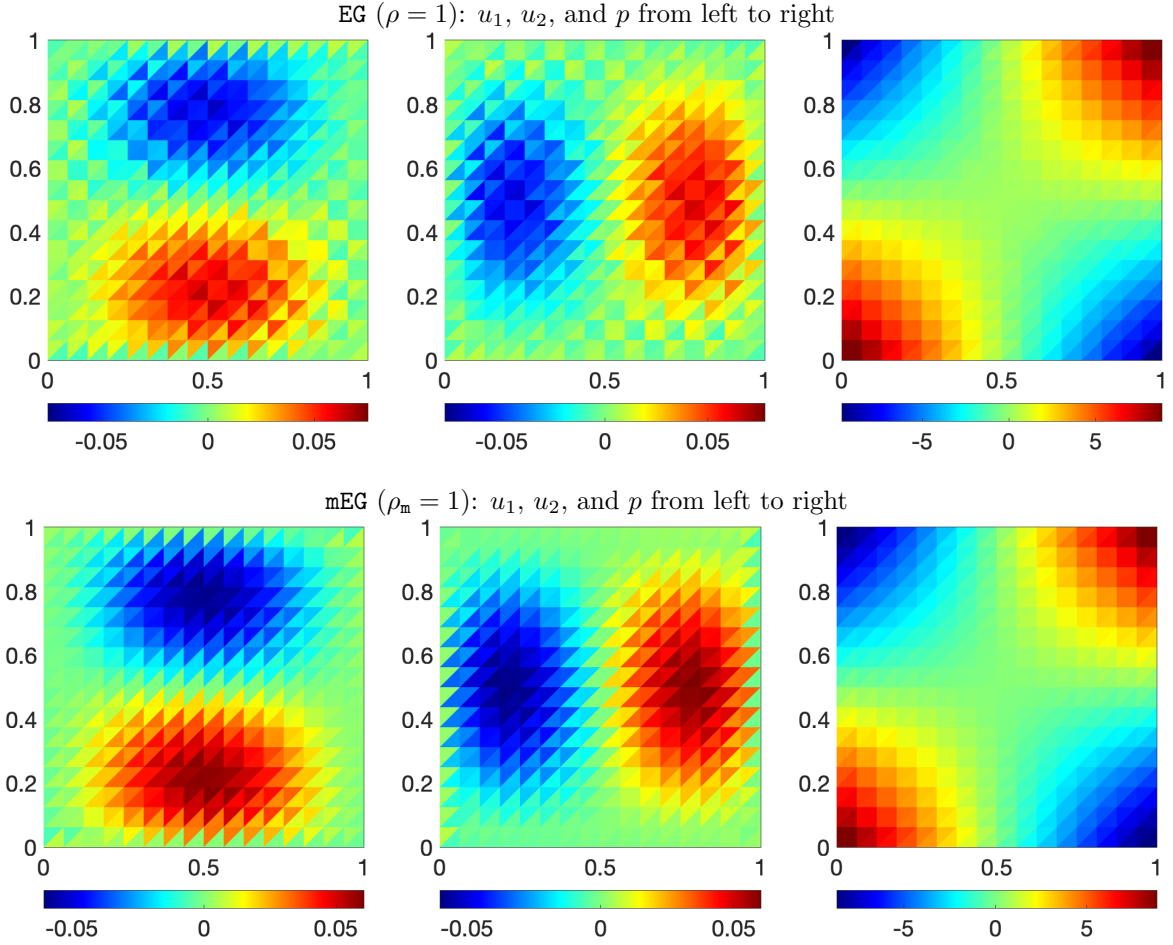


Figure 2: Comparison of the numerical solutions with  $h = 1/16$  and  $\nu = 1$ .

- **Perturbed mesh:** The uniform triangular mesh is randomly perturbed, so some very sharp triangles are generated. The velocity field and pressure in (6.5) are considered. The homogeneous boundary condition is preserved.
- **Square with hole:** The computational domain is the unit square with a hole in the middle. An adaptive mesh is generated with triangles of different sizes. The velocity field and pressure in (6.5) are considered. The homogeneous boundary condition is preserved on the outer square, but a non-homogeneous boundary condition occurs on the circle in the middle.
- **L-shape:** The computational domain is the L-shaped domain, and it is discretized with quasi-uniform triangles. The velocity field and pressure are chosen as  $\mathbf{u}(x, y) = (\sin(\pi x) \sin(\pi y), \cos(\pi x) \cos(\pi y))$  and  $p(x, y) = |y|$ .

Figure 3 shows the above meshes, the corresponding mesh qualities, and the velocity errors with different penalty parameters. The mesh quality of a triangle [8] is defined as the ratio of its area to the sum of the squares of its sides, which implies that the equilateral triangle has the best mesh quality 1 and sharper triangles are closer to 0. For the EG method, sufficiently large penalty parameters are required to achieve a desired accuracy. Moreover, such large parameters are depending on the meshes. To be specific, in **Perturbed mesh**, some bad quality triangles cause an unexpected spike around  $\rho = 3$  in the velocity errors, which makes it more difficult to choose a proper penalty parameter. However, on all the given meshes, the mEG method seems uniformly stable with any positive penalty parameter. The mEG method, even for the mesh with bad quality triangles, has good performance. These numerical results confirm that the mEG method is a parameter-free scheme.

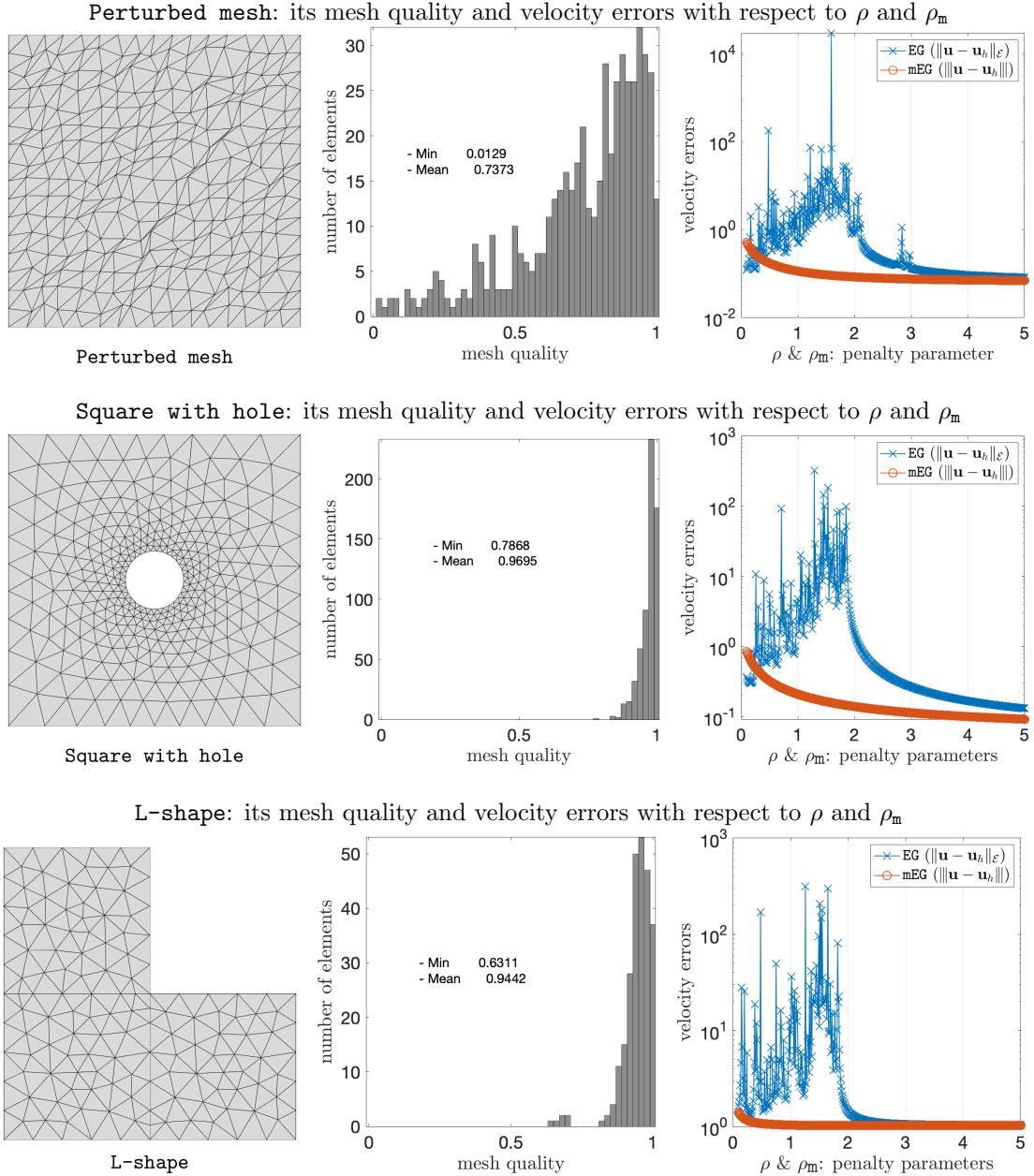


Figure 3: Comparison of EG and mEG for  $0.1 \leq \rho, \rho_m \leq 5$  on various meshes ( $\nu = 1$ ).

### 6.1.2 Pressure-robustness test

In this test, we verify the pressure-robustness of the PR-mEG method. We solve the example problem (6.5) with varying  $\nu$ , from  $10^{-2}$  to  $10^{-6}$ , to confirm the error behaviors expected in (6.3) and (6.4). The mesh size is fixed as  $h = 1/32$ . Figure 4 shows the velocity errors  $\|\mathbf{u} - \mathbf{u}_h\|$  and pressure errors  $\|\mathcal{P}_0 p - p_h\|_0$  of the mEG and PR-mEG methods. In Figure 4, the mEG method produces the velocity errors proportional to  $\nu^{-1}$  because the second term  $h\nu^{-1}\|p\|_1$  of the error bound (6.3b) becomes dominant as  $\nu$  gets smaller. Also, since the pressure error  $\|\mathcal{P}_0 p - p_h^{\text{mEG}}\|_0$  is bounded by a dominant term  $h\|p\|_1$ , the error remains the same. On the other hand, the PR-mEG method produces the same velocity errors regardless of  $\nu$ , and its pressure errors decrease in proportion to  $\nu$ . These numerical results support our theoretical error estimates related to the pressure-robustness in (6.3) and (6.4).

Furthermore, we perform a mesh refinement study for the mEG and PR-mEG methods with decreasing mesh size  $h$  and fixed  $\nu = 10^{-6}$ . As shown in Table 2, the velocity and pressure errors for both methods decrease in at least the first order of convergence, and the pressure errors look very similar in magnitude. However, even though the velocity errors for the mEG method decrease at a faster rate, the magnitude of the errors seems huge. Thus, it may not be possible to obtain accurate numerical velocity from the mEG

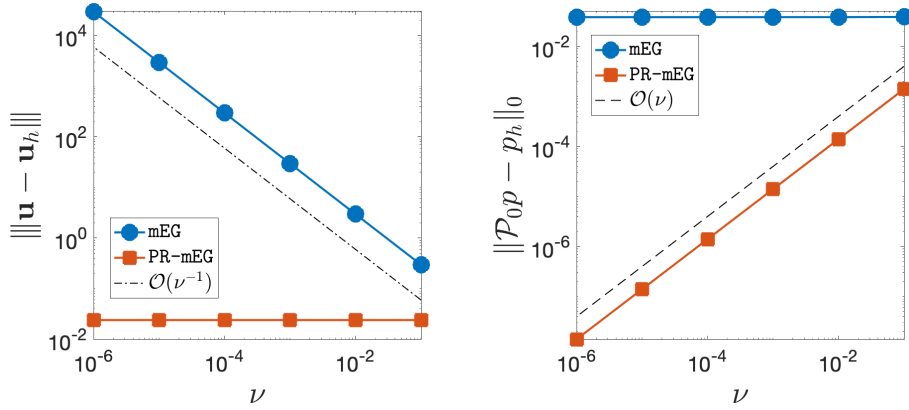


Figure 4: Error profiles of the mEG and PR-mEG methods with varying  $\nu$  values and a fixed mesh size  $h = 1/32$ .

$h$	mEG		PR-mEG	
	$\ u - u_h^{\text{mEG}}\ _0$	Rate	$\ u - u_h^{\text{PR}}\ _0$	Rate
1/8	2.577e+5	-	9.727e-2	-
1/16	9.097e+4	1.50	4.749e-2	1.03
1/32	3.183e+4	1.52	2.339e-2	1.02
1/64	1.116e+4	1.51	1.159e-2	1.01
$h$	$\ p - p_h^{\text{mEG}}\ _0$	Rate	$\ p - p_h^{\text{PR}}\ _0$	Rate
1/8	5.736e-1	-	4.802e-1	-
1/16	2.694e-1	1.09	2.404e-1	1.00
1/32	1.310e-1	1.04	1.203e-1	1.00
1/64	6.464e-2	1.02	6.014e-2	1.00

Table 2: A mesh refinement study for mEG and PR-mEG with varying mesh size  $h$  and  $\nu = 10^{-6}$ .

method unless  $h$  is small enough. On the other hand, the PR-mEG method yields about a million times smaller velocity errors than the mEG method. This means that the PR-mEG method provides a significantly improved numerical velocity for the Stokes equations with small viscosity, which is an important feature of pressure-robust numerical schemes.

## 6.2 Three dimensional examples

We consider a 3D flow in a unit cube  $\Omega = (0, 1)^3$ . The velocity field and pressure are chosen as

$$\mathbf{u} = \begin{pmatrix} \sin(\pi x) \cos(\pi y) - \sin(\pi x) \cos(\pi z) \\ \sin(\pi y) \cos(\pi z) - \sin(\pi y) \cos(\pi x) \\ \sin(\pi z) \cos(\pi x) - \sin(\pi z) \cos(\pi y) \end{pmatrix}, \quad p = \sin(\pi x) \sin(\pi y) \sin(\pi z). \quad (6.6)$$

### 6.2.1 Parameter-free test

In this example, with different penalty parameters, we compute the velocity and pressure errors and condition numbers in the EG and mEG methods. Figure 5 clearly shows the need of a sufficiently large penalty parameter for the EG method and the stability of the mEG method with any positive parameter. Figure 6 also displays the magnitudes of the numerical velocity of the EG and mEG methods with  $\rho = \rho_m = 1$ . Although both methods give similar color patterns, some sharp changes in color occur in the velocity of the EG method. The sharp changes are caused by the insufficiently large parameter, and they make the numerical velocity inaccurate.

In addition, we focus on the effect of large penalty parameters on the errors and condition numbers. In Figure 5, the condition numbers of both methods tend to increase with the parameters  $\rho$  and  $\rho_m$ , which causes the increased velocity and pressure errors. In order to perform quantitative comparison, we choose  $\rho = 10$  and  $\rho = 2$  based on the results in Figure 5 and report the pressure and velocity errors of the two cases in Table 3. The pressure errors of the EG method with  $\rho = 10$  are 10 times bigger



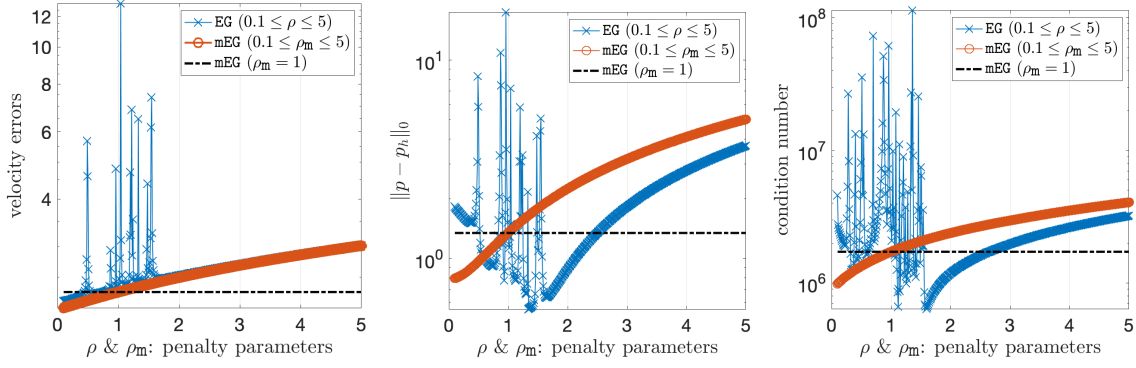


Figure 5: Errors and condition numbers of EG and mEG for  $0.1 \leq \rho \leq 5$  ( $\nu = 1$ ,  $h = 1/4$ ) in the 3D case.

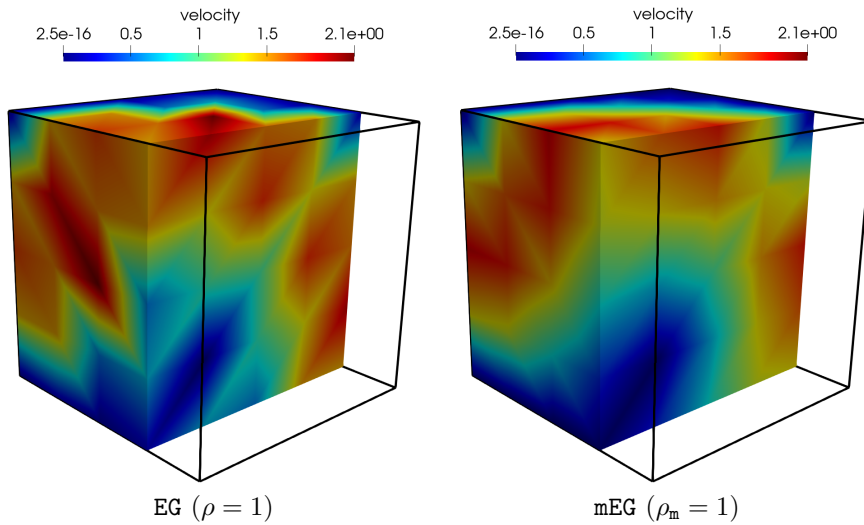


Figure 6: Comparison of 3D numerical velocity solutions when  $h = 1/4$  and  $\nu = 1$ .

than those with  $\rho = 2$ , even though their pressure errors decrease at the same rate. Thus, in practice, a penalty parameter  $\rho$  cannot be chosen too large due to this accuracy issue. It may also be challenging to choose a proper  $\rho$  because it varied with meshes. On the other hand, for the mEG method with  $\rho_m = 1$ , the convergence rates of the velocity and pressure errors are of at least first-order, and the mEG method yields smaller velocity errors than the EG method with  $\rho = 2$ . Therefore, with the mEG method, we can always safely choose  $\rho_m = 1$  to achieve reliable performance, so we can make the simulation lower-cost.

### 6.2.2 Pressure-robust test

To verify the pressure-robustness in the three-dimensional example (6.6), we consider the pattern of the error behaviors obtained from the mEG and PR-mEG methods when  $\nu$  varies and the mesh size is fixed to  $h = 1/16$ . In Figure 7, we observe the same error behaviors as those in the two dimensional pressure-robust test. That is, for the mEG method, the velocity errors are inversely proportional to  $\nu$  while the pressure errors tend to stay constant. On the other hand, for the PR-mEG method, the velocity errors seem independent of  $\nu$ , and the pressure errors decrease in proportion to  $\nu$ .

Furthermore, Figure 8 shows the streamlines of the velocity solutions of the mEG and PR-mEG methods when  $h = 1/8$  and  $\nu = 10^{-6}$ . In this case, the velocity error of the mEG method is  $1.014e+4$  while that of the PR-mEG method is  $1.122e+0$ . As shown in Figure 8, the numerical velocity of the PR-mEG method well captures the 3D vortex flow, while that of the mEG method is unable to do so.

## 7 Conclusion

In this paper, we proposed a low-cost, parameter-free, and pressure-robust Stokes solver based on the EG method operating with minimal degrees of freedom. The weak derivatives, simply computed by the

$h$	EG ( $\rho = 10$ )		EG ( $\rho = 2$ )		mEG ( $\rho_m = 1$ )	
	$\ \mathbf{u} - \mathbf{u}_h^{\text{EG}}\ _{\mathcal{E}}$	Rate	$\ \mathbf{u} - \mathbf{u}_h^{\text{EG}}\ _{\mathcal{E}}$	Rate	$\ \mathbf{u} - \mathbf{u}_h^{\text{mEG}}\ $	Rate
1/4	3.719e+0	-	2.518e+0	-	2.284e+0	-
1/8	1.827e+0	1.03	1.228e+0	1.04	1.121e+0	1.03
1/16	9.048e-1	1.01	6.052e-1	1.02	5.552e-1	1.01
1/32	4.501e-1	1.01	3.007e-1	1.01	2.764e-1	1.01
$h$	$\ p - p_h^{\text{EG}}\ _0$	Rate	$\ p - p_h^{\text{EG}}\ _0$	Rate	$\ p - p_h^{\text{mEG}}\ _0$	Rate
1/4	8.377e+0	-	8.819e-1	-	1.349e+0	-
1/8	3.600e+0	1.22	3.611e-1	1.29	6.098e-1	1.15
1/16	1.670e+0	1.11	1.688e-1	1.10	3.011e-1	1.02
1/32	8.312e-1	1.01	8.411e-2	1.00	1.504e-1	1.00

Table 3: A mesh refinement study for EG and mEG with varying mesh size  $h$  and  $\nu = 1$  in the 3D case.

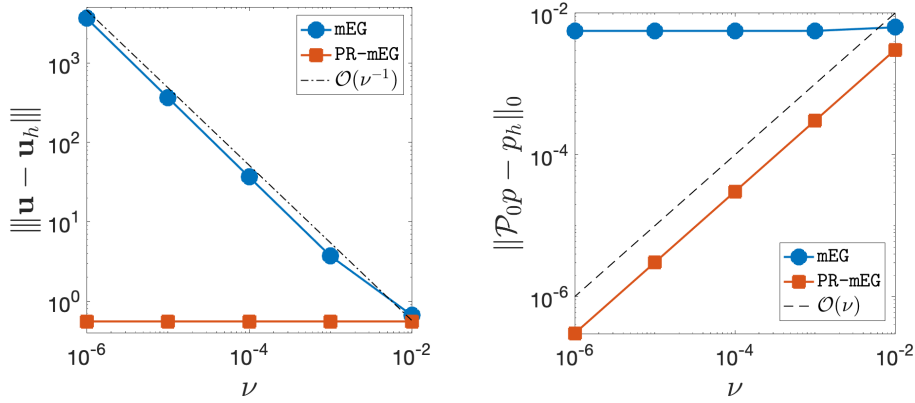


Figure 7: Error profiles of the mEG and PR-mEG methods with varying  $\nu$  values and a fixed mesh size  $h = 1/16$  in the 3D case.

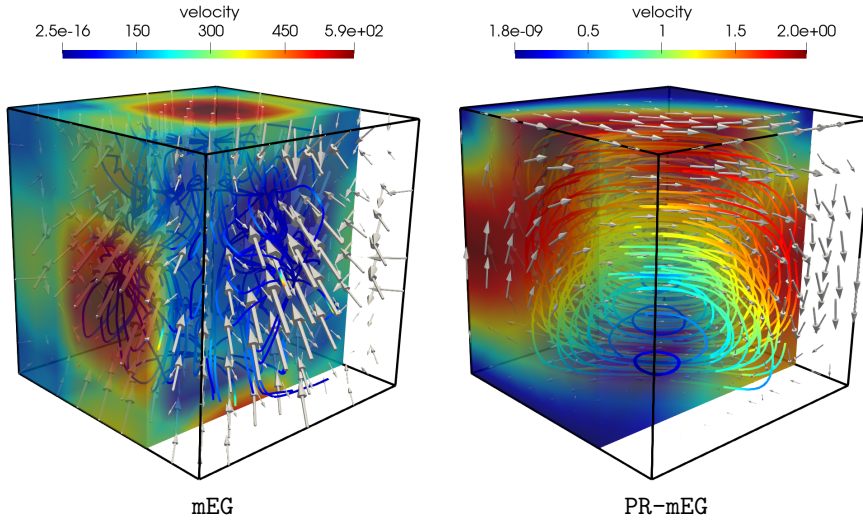


Figure 8: Streamlines of the 3D numerical velocity when  $h = 1/8$  and  $\nu = 10^{-6}$ .

geometric data of elements, allowed the EG method to be free of penalty parameters and some IPDG trace terms. With reduced computational complexity, the modified EG method preserved the minimal degrees of freedom and the optimal rates in convergence of the EG method. Furthermore, we achieved the pressure-robustness for the modified EG method by the simple modification on the right-hand side. We also confirmed the improved theoretical results through the several numerical tests with two- and three-dimensional examples. The idea of using weak derivatives can be applied to improve other numerical schemes employing the symmetric IPDG formulation. The extension of the idea to numerical schemes for the biharmonic equation will be one of our future research directions. We expect that the weak

derivatives corresponding to the biharmonic equation provide significant computational advantages in solving application problems involving the biharmonic equation numerically.

## References

- [1] Mark Ainsworth. A posteriori error estimation for discontinuous Galerkin finite element approximation. *SIAM Journal on Numerical Analysis*, 45(4):1777–1798, 2007.
- [2] Mark Ainsworth and Richard Rankin. Fully computable error bounds for discontinuous Galerkin finite element approximations on meshes with an arbitrary number of levels of hanging nodes. *SIAM Journal on Numerical Analysis*, 47(6):4112–4141, 2010.
- [3] Ivo Babuška. The finite element method with Lagrangian multipliers. *Numerische Mathematik*, 20(3):179–192, 1973.
- [4] Christine Bernardi and Genevieve Raugel. Analysis of some finite elements for the Stokes problem. *Mathematics of Computation*, 44(169):71–79, 1985.
- [5] Susanne C Brenner and Li-Yeng Sung.  $C^0$  interior penalty methods for fourth order elliptic boundary value problems on polygonal domains. *Journal of Scientific Computing*, 22(1):83–118, 2005.
- [6] Franco Brezzi. On the existence, uniqueness and approximation of saddle-point problems arising from Lagrangian multipliers. *Publications mathématiques et informatique de Rennes*, (S4):1–26, 1974.
- [7] Nabil Chaabane, Vivette Girault, Béatrice Rivière, and Travis Thompson. A stable enriched Galerkin element for the Stokes problem. *Applied Numerical Mathematics*, 132:1–21, 2018.
- [8] Long Chen. Mesh smoothing schemes based on optimal Delaunay triangulations. In *IMR*, pages 109–120, 2004.
- [9] Long Chen. *iFEM: An Integrated Finite Element Methods Package in MATLAB*. Technical Report, University of California at Irvine, 2009.
- [10] Bernardo Cockburn, Jayadeep Gopalakrishnan, and Raytcho Lazarov. Unified hybridization of discontinuous Galerkin, mixed, and continuous Galerkin methods for second order elliptic problems. *SIAM Journal on Numerical Analysis*, 47(2):1319–1365, 2009.
- [11] Michel Crouzeix and P-A Raviart. Conforming and nonconforming finite element methods for solving the stationary Stokes equations I. *Revue française d’automatique informatique recherche opérationnelle. Mathématique*, 7(R3):33–75, 1973.
- [12] Daniele A Di Pietro and Alexandre Ern. Hybrid high-order methods for variable-diffusion problems on general meshes. *Comptes Rendus Mathématique*, 353(1):31–34, 2015.
- [13] Yekaterina Epshteyn and Béatrice Rivière. Estimation of penalty parameters for symmetric interior penalty Galerkin methods. *Journal of Computational and Applied Mathematics*, 206(2):843–872, 2007.
- [14] Nicolas R Gauger, Alexander Linke, and Philipp W Schroeder. On high-order pressure-robust space discretisations, their advantages for incompressible high Reynolds number generalised Beltrami flows and beyond. *The SMAI Journal of Computational Mathematics*, 5:89–129, 2019.
- [15] Vivette Girault, Béatrice Rivière, and Mary F. Wheeler. A discontinuous Galerkin method with nonoverlapping domain decomposition for the Stokes and Navier-Stokes problems. *Mathematics of Computation*, 74(249):53–84, 2005.
- [16] Peter Hansbo and Mats G. Larson. Piecewise divergence-free discontinuous Galerkin methods for Stokes flow. *Communications in Numerical Methods in Engineering*, 24(5):355–366, 2008.
- [17] Xiaozhe Hu, Seulip Lee, Lin Mu, and Son-Young Yi. Pressure-robust enriched Galerkin methods for the Stokes equations. *arXiv:2208.13076*, 2022.

- [18] Olga Aleksandrovna Ladyzhenskaya. *The Mathematical Theory of Viscous Incompressible Flow*, volume 2. Gordon and Breach New York, 1969.
- [19] Sanghyun Lee, Young-Ju Lee, and Mary F Wheeler. A locally conservative enriched Galerkin approximation and efficient solver for elliptic and parabolic problems. *SIAM Journal on Scientific Computing*, 38(3):A1404–A1429, 2016.
- [20] Yuwen Li and Ludmil T Zikatanov. New stabilized  $P_1 \times P_0$  finite element methods for nearly inviscid and incompressible flows. *Computer Methods in Applied Mechanics and Engineering*, 393:114815, apr 2022.
- [21] Alexander Linke. A divergence-free velocity reconstruction for incompressible flows. *Comptes Rendus Mathematique*, 350(17-18):837–840, 2012.
- [22] Alexander Linke and Christian Merdon. Pressure-robustness and discrete Helmholtz projectors in mixed finite element methods for the incompressible Navier–Stokes equations. *Computer Methods in Applied Mechanics and Engineering*, 311:304–326, 2016.
- [23] Lin Mu. Pressure robust weak Galerkin finite element methods for Stokes problems. *SIAM Journal on Scientific Computing*, 42(3):B608–B629, 2020.
- [24] Lin Mu, Xiaoshen Wang, and Xiu Ye. A modified weak Galerkin finite element method for the Stokes equations. *Journal of Computational and Applied Mathematics*, 275:79–90, 2015.
- [25] Lin Mu, Junping Wang, Xiu Ye, and Shangyou Zhang. A discrete divergence free weak Galerkin finite element method for the Stokes equations. *Applied Numerical Mathematics*, 125:172–182, 2018.
- [26] Lin Mu, Xiu Ye, and Shangyou Zhang. Development of pressure-robust discontinuous Galerkin finite element methods for the Stokes problem. *Journal of Scientific Computing*, 89(1):1–25, 2021.
- [27] Shuyu Sun and Jianguo Liu. A locally conservative finite element method based on piecewise constant enrichment of the continuous Galerkin method. *SIAM Journal on Scientific Computing*, 31(4):2528–2548, 2009.
- [28] C. Taylor and P. Hood. A numerical solution of the Navier-Stokes equations using the finite element technique. *Computers & Fluids*, 1(1):73–100, 1973.
- [29] Junping Wang and Xiu Ye. A weak Galerkin finite element method for second-order elliptic problems. *Journal of Computational and Applied Mathematics*, 241:103–115, 2013.
- [30] Junping Wang and Xiu Ye. A weak Galerkin finite element method for the Stokes equations. *Advances in Computational Mathematics*, 42(1):155–174, 2016.
- [31] Xiaoshen Wang, Nolisa S Malluwawadu, Fuzheng Gao, and TC McMillan. A modified weak Galerkin finite element method. *Journal of Computational and Applied Mathematics*, 271:319–327, 2014.
- [32] Yingying Xie, Shuhao Cao, Long Chen, and Liuqiang Zhong. Convergence and optimality of an adaptive modified weak Galerkin finite element method. *arXiv:2007.12853*, 2020.
- [33] Son-Young Yi, Xiaozhe Hu, Sanghyun Lee, and James H. Adler. An enriched Galerkin method for the Stokes equations. *Computers and Mathematics with Applications*, 120:115–131, 2022.
- [34] Son-Young Yi, Sanghyun Lee, and Ludmil T Zikatanov. Locking-free enriched Galerkin method for linear elasticity. *SIAM Journal on Numerical Analysis*, 60(1):52–75, 2022. ISSN 0036-1429.
- [35] Lina Zhao, Eun-Jae Park, and Eric Chung. A pressure robust staggered discontinuous Galerkin method for the Stokes equations. *Computers & Mathematics with Applications*, 128:163–179, 2022.